

## Space-time evolution of nuclear reactions probed by two-proton intensity interferometry

W. G. Gong, W. Bauer, and C. K. Gelbke

*National Superconducting Cyclotron Laboratory and Department of Physics and Astronomy, Michigan State University,  
East Lansing, Michigan 48824*

S. Pratt

*Department of Physics, University of Wisconsin, Madison, Wisconsin 53706*

(Received 24 September 1990)

An approximate relation is derived which allows the calculation of the two-proton correlation function for any reaction model capable of predicting the classical single-particle phase-space distribution or Wigner function in the exit channel. The sensitivity of the calculated two-proton correlation functions to source radii and lifetimes is illustrated with simple parametrizations. More realistic calculations are presented for two different regimes of emission time scales: slow particle evaporation from equilibrated compound nuclei, as predicted from the Weisskopf formula, and fast nonequilibrium particle emission in intermediate-energy nucleus-nucleus collisions, as predicted from the Boltzmann-Uehling-Uhlenbeck transport equation.

### I. INTRODUCTION

Two particles, emitted at small relative momenta from an excited nuclear system, carry information about the space-time characteristics of the emitting source.<sup>1-24</sup> The shape of two-proton correlation function reflects the interplay of the short-range nuclear interaction, the Pauli exclusion principle, and the long-range Coulomb interaction between the two emitted protons.<sup>1,2,14</sup> The attractive *S*-wave nuclear interaction leads to a pronounced maximum in the two-proton correlation function at relative momentum  $q \approx 20 \text{ MeV}/c$ , when the average distance upon emission is of the order of 10 fm or less.<sup>1</sup> The long-range Coulomb interaction and the Pauli exclusion principle give rise to a minimum at  $q = 0$ . Some directional information can be provided by antisymmetrization effects<sup>2,14,16</sup> when  $|q \cdot r| < \hbar$ , where  $q$  and  $r$  denote the relative momentum and position vectors upon emission.

In this article, we give a brief derivation of the general formalism which allows the calculation of two-proton correlation functions from the knowledge of the single-particle phase-space density. The sensitivity of two-proton correlation functions to source radii and lifetimes is illustrated by means of simple analytical source parametrizations. Different regimes of emission time scales are explored by giving specific examples for slow evaporative and fast nonevaporative particle emission processes, calculated with the Weisskopf evaporation formula and the Boltzmann-Uehling-Uhlenbeck (BUU) transport equation, respectively.

The paper is structured as follows. In Sec. II, we present a brief derivation of the general formalism which relates the two-proton correlation function to the single-particle Wigner function. In Sec. III, we illustrate the sensitivity of two-proton correlation functions to source

radii and emission time scales by performing calculations for a number of simple source parametrizations. In Sec. IV, we give a brief review of the basic assumptions underlying the derivation of the BUU transport equation. Numerical results obtained by solving the BUU equation are presented in Sec. V. Sec. VI gives a brief review of the Weisskopf formula used for the calculation of particle evaporation from equilibrated compound nuclei; numerical results are given in Sec. VII. A summary is given in Sec. VIII. Detailed comparisons with recent experimental results will be given in a forthcoming paper.<sup>24</sup>

### II. CORRELATION FUNCTION FORMALISM

A number of formalisms have been published<sup>1</sup> which derive two-particle correlation functions from the knowledge of the emission function  $g(\mathbf{p}, x)$ , i.e., the probability of emitting a particle with momentum  $\mathbf{p}$  from space-time point  $x = (\mathbf{r}, t)$ . The derived expressions differ only in minor details and the predicted results are similar. Here, we derive an expression for the correlation function in most general terms, assuming complete knowledge of all two-particle quantum-mechanical matrix elements. We then introduce and justify approximations which allow practical calculations. For simplicity, we will restrict ourselves to the important case of correlations between two identical particles.

In the following, we will use four-vector notation to keep our formulas compact and manageable. However, our formalism is not relativistically covariant.

Our final expression for the two-particle correlation function is identical to the expression given in Refs. 2 and 14:

$$\begin{aligned}
R(\mathbf{P}, \mathbf{q}) + 1 &= C(\mathbf{P}, \mathbf{q}) \\
&= \frac{\Pi(\mathbf{p}_1, \mathbf{p}_2)}{\Pi(\mathbf{p}_1)\Pi(\mathbf{p}_2)} \\
&= \frac{\int d^4x_1 d^4x_2 g(\mathbf{P}/2, x_1) g(\mathbf{P}/2, x_2) |\phi(\mathbf{q}, \mathbf{r}_1 - \mathbf{r}_2 - (t_2 - t_1)\mathbf{P}/2m)|^2}{\int d^4x_1 g(\mathbf{P}/2, x_1) \int d^4x_2 g(\mathbf{P}/2, x_2)} \quad (1)
\end{aligned}$$

Here,  $\Pi(\mathbf{p}_1, \mathbf{p}_2)$  and  $\Pi(\mathbf{p})$  denote the two-particle and single-particle emission probabilities,  $\mathbf{P}$  and  $\mathbf{q}$  are the total and relative momenta,  $\mathbf{P} = \mathbf{p}_1 + \mathbf{p}_2$  and  $\mathbf{q} = (\mathbf{p}_1 - \mathbf{p}_2)/2$ , respectively, and  $\phi$  is the relative wave function.

This expression was given in Ref. 2 without derivation. It was derived in Ref. 14 by using the sudden approximation for which the particles are assumed to be on shell in their final state and the mutual interaction is switched on suddenly. Equation (1) was then derived assuming the thermal wavelength is much smaller than the size of the system. These approximations are not very well justified. Here, we start from the full quantum-mechanical expression for two-particle emission and show how, under most circumstances, we can justify a few approximations which lead to Eq. (1). Results obtained in many other formalisms are similar. For instance, in the literature on two-pion interferometry the function  $g(\mathbf{P}/2, x)$  is often replaced by something similar, for example,  $[g(\mathbf{p}_1, x) \cdot g(\mathbf{p}_2, x)]^{1/2}$ . As long as the relative momentum  $|\mathbf{q}|$  is much smaller than a characteristic momentum  $|\mathbf{p}|$  of  $g(\mathbf{p}, x)$  (such as  $|\mathbf{p}| \approx \sqrt{3mT}$ , where  $T$  is the temperature), there is little difference between the formalisms.

The complete matrix element for the creation of the  $n$ -body final state includes all information necessary for the calculation of correlation functions. Here we will derive an approximation in which the correlation function will only depend on properties of the one-body emission probability which can be extracted from the one-body matrix elements.

We start out by first considering the probability for creating two particles with final momenta  $\mathbf{p}_1$  and  $\mathbf{p}_2$  from sources 1 and 2 at space-time points  $x_1$  and  $x_2$ :

$$\begin{aligned}
\Pi(\mathbf{p}_1, \mathbf{p}_2) &= \left| \int d^4x_1 d^4x_2 M_1(x_1) M_2(x_2) U(x_1, x_2; \mathbf{p}_1, \mathbf{p}_2) \right|^2 \quad (2)
\end{aligned}$$

Here,  $U(x_1, x_2; \mathbf{p}_1, \mathbf{p}_2)$  is the evolution operator for particles created at  $x_1$  and  $x_2$  which end up in the asymptotic momentum states  $\mathbf{p}_1$  and  $\mathbf{p}_2$ . The matrix element  $M_i(x_i)$  creates the particle at  $x_i$  and the remaining collision products into a state which henceforth does not interact with the particle. In Eq. (2), we have assumed that the particles are emitted independently. This allows the factorization of the matrix element for two-body emission into the product of single-body elements.

By squaring the matrix elements and transforming to the new coordinates  $x_i$  (mean) and  $\delta x_i$  (relative), we obtain

$$\begin{aligned}
\Pi(\mathbf{p}_1, \mathbf{p}_2) &= \int d^4x_1 d^4\delta x_1 d^4x_2 d^4\delta x_2 S_1(x_1, \delta x_1) \\
&\quad \times S_2(x_2, \delta x_2) \bar{W}_{\mathbf{p}_1, \mathbf{p}_2}(x_1, \delta x_1, x_2, \delta x_2), \quad (3)
\end{aligned}$$

where

$$\begin{aligned}
W_{\mathbf{p}_1, \mathbf{p}_2}(x_1, \delta x_1, x_2, \delta x_2) &= U^\dagger(x_1 + \delta x_1/2, x_2 + \delta x_2/2; \mathbf{p}_1, \mathbf{p}_2) \\
&\quad \times U(x_1 - \delta x_1/2, x_2 - \delta x_2/2; \mathbf{p}_1, \mathbf{p}_2), \quad (4)
\end{aligned}$$

and

$$S_1(x_1, \delta x_1) = M_1^\dagger(x_1 + \delta x_1/2) M_1(x_1 - \delta x_1/2). \quad (5)$$

The expression becomes physically more transparent when the dependences on  $\delta x_i$  are replaced by dependences on the momenta  $k_i$  through four-dimensional Wigner transforms. As a result, we obtain

$$\begin{aligned}
\Pi(\mathbf{p}_1, \mathbf{p}_2) &= \int d^4x_1 d^4x_2 d^4k_1 d^4k_2 \bar{S}_1(x_1, k_1) \\
&\quad \times \bar{S}_2(x_2, k_2) \bar{W}_{\mathbf{p}_1, \mathbf{p}_2}(x_1, k_1, x_2, k_2), \quad (6)
\end{aligned}$$

with the Wigner transforms  $\bar{S}$  and  $\bar{W}$  defined by

$$\bar{S}_i(x, k) = \int d^4\delta x S_i(x, \delta x) e^{i\delta x \cdot k}, \quad (7)$$

and

$$\begin{aligned}
\bar{W}_{\mathbf{p}_1, \mathbf{p}_2}(x_1, k_1, x_2, k_2) &= \int d^4\delta x_1 d^4\delta x_2 W_{\mathbf{p}_1, \mathbf{p}_2}(x_1, \delta x_1, x_2, \delta x_2) \\
&\quad \times e^{-i\delta x_1 \cdot k_1 - i\delta x_2 \cdot k_2}. \quad (8)
\end{aligned}$$

For noninteracting distinguishable particles, the time-evolution operators  $U$  in Eq. (2) become simple exponentials, and we obtain from Eq. (4) the relation  $W_{\mathbf{p}_1, \mathbf{p}_2} = \exp(i\delta x_1 \cdot \mathbf{p}_1 + i\delta x_2 \cdot \mathbf{p}_2)$ . In this case, we can see from Eq. (8) that

$$\bar{W}_{\mathbf{p}_1, \mathbf{p}_2}(x_1, k_1, x_2, k_2) = \delta^4(\mathbf{p}_1 - k_1) \delta^4(\mathbf{p}_2 - k_2),$$

as expected: Noninteracting distinguishable particles retain their four-momentum after the emission.

The functions  $\bar{S}_i(x, k)$  are the quantum-mechanical analogs of the emission probability for particles with four-momentum  $k$  from space-time point  $x$ . This can be seen from the following argument. Performing the same steps as above, but now for the single-particle distributions, and making use of the relation  $\bar{W}_{\mathbf{p}}(x, k) = \delta^4(p - k)$ , we obtain the result

$$\Pi(\mathbf{p}) = \int d^4x d^4k \bar{S}(x, k) \delta^4(p - k). \quad (9)$$

From here on, we will imply the on-shell condition  $p^0 = E(\mathbf{p})$  when referring to the zeroth component of the asymptotic momentum. Equation (9) shows that the emission probability is given by

$$g(\mathbf{p}, \mathbf{x}) = \bar{S}(x, p). \quad (10)$$

In order to obtain an expression for  $\bar{W}_{\mathbf{p}_1, \mathbf{p}_2}(x_1, k_1, x_2, k_2)$ , we assume that the first emitted particle propagates freely for a time  $t_2 - t_1$  before it interacts with the second particle which is created at  $t_2$ . With this assumption, the evolution operator,

$$\begin{aligned} \bar{U}(\mathbf{k}_1, t_1, \mathbf{k}_2, t_2; \mathbf{p}_1, \mathbf{p}_2) \\ = (2\pi)^{-6} \int d^3x_1 d^3x_2 U(x_1, x_2; \mathbf{p}_1, \mathbf{p}_2) \\ \times e^{-ik_1 \cdot x_1 - ik_2 \cdot x_2}, \end{aligned} \quad (11)$$

for momentum states  $\mathbf{k}_i$ , to evolve into the true scattering states  $\mathbf{p}_i$ , can be written as

$$\begin{aligned} \bar{U}(\mathbf{k}_1, t_1, \mathbf{k}_2, t_2; \mathbf{p}_1, \mathbf{p}_2) \\ = \Phi(\mathbf{k}_1, \mathbf{k}_2; \mathbf{p}_1, \mathbf{p}_2) \exp[iE_{12}t_2 + iE_1(t_1 - t_2)]. \end{aligned} \quad (12)$$

Here  $E_{12}$  is the total kinetic energy of the proton pair, and  $\Phi$  is the projection of the total wave function on the plane-wave states  $\mathbf{k}_1$  and  $\mathbf{k}_2$ .

If the emissions of the two particles are not far apart in time, the assumption of time-ordered emission entering Eq. (12) becomes questionable due to the uncertainty principle.

One can now calculate  $\bar{W}$  in terms of the wave-function projection  $\Phi$ :

$$\begin{aligned} \bar{W}_{\mathbf{p}_1, \mathbf{p}_2}(x_1, k_1, x_2, k_2) = \int d\delta t_1 d^3\delta\mathbf{k}_1 d\delta t_2 d^3\delta\mathbf{k}_2 \bar{U}^\dagger(\mathbf{k}_1 + \delta\mathbf{k}_1/2, t_1 + \delta t_1/2, \mathbf{k}_2 + \delta\mathbf{k}_2/2, t_2 + \delta t_2/2; \mathbf{p}_1, \mathbf{p}_2) \\ \times \bar{U}(\mathbf{k}_1 - \delta\mathbf{k}_1/2, t_1 - \delta t_1/2, \mathbf{k}_2 - \delta\mathbf{k}_2/2, t_2 - \delta t_2/2; \mathbf{p}_1, \mathbf{p}_2) \\ \times \exp(-ik_1^0 \delta t_1 - ik_2^0 \delta t_2 - i\delta\mathbf{k}_1 \cdot \mathbf{x}_1 - i\delta\mathbf{k}_2 \cdot \mathbf{x}_2) \\ = \int d^3\delta k_1 d^3\delta k_2 d^3R_1 d^3R_2 \delta(k_1^0 - E_1) \delta(k_2^0 - (E_{12} - E_1)) f_2(\mathbf{k}_1, \mathbf{k}_2, \mathbf{R}_1, \mathbf{R}_2; \mathbf{p}_1, \mathbf{p}_2) \\ \times e^{-i\delta\mathbf{k}_1 \cdot (\mathbf{x}_1 + \mathbf{k}_1(t_2 - t_1)/m - \mathbf{R}_1) - i\delta\mathbf{k}_2 \cdot (\mathbf{x}_2 - \mathbf{R}_2)}. \end{aligned} \quad (13)$$

Here, the symbol  $k_i^0$  is the zeroth component of the four-vector  $k_i$ . To arrive at the second part of Eq. (13), we performed Fourier transforms and made the linear approximation for the energy,  $E(\mathbf{k} + \delta\mathbf{k}) \approx E(\mathbf{k}) + \delta\mathbf{k} \cdot \mathbf{k}/m$ . The function  $f_2$  introduced into Eq. (13) is the Wigner decomposition of the total two-particle density matrix:

$$\begin{aligned} f_2(\mathbf{k}_1, \mathbf{k}_2, \mathbf{R}_1, \mathbf{R}_2; \mathbf{p}_1, \mathbf{p}_2) = \int d^3\delta k_1 d^3\delta k_2 \exp(-i\delta\mathbf{k}_1 \cdot \mathbf{R}_1 - i\delta\mathbf{k}_2 \cdot \mathbf{R}_2) \\ \times \Phi^*(\mathbf{k}_1 + \delta\mathbf{k}_1/2, \mathbf{k}_2 + \delta\mathbf{k}_2/2; \mathbf{p}_1, \mathbf{p}_2) \Phi(\mathbf{k}_1 - \delta\mathbf{k}_1/2, \mathbf{k}_2 - \delta\mathbf{k}_2/2; \mathbf{p}_1, \mathbf{p}_2) \\ = \int d^3\delta x_1 d^3\delta x_2 \exp(-i\delta\mathbf{x}_1 \cdot \mathbf{k}_1 - i\delta\mathbf{x}_2 \cdot \mathbf{k}_2) \\ \times \Phi^*(\mathbf{R}_1 + \delta\mathbf{x}_1/2, \mathbf{R}_2 + \delta\mathbf{x}_2/2; \mathbf{p}_1, \mathbf{p}_2) \Phi(\mathbf{R}_1 - \delta\mathbf{x}_1/2, \mathbf{R}_2 - \delta\mathbf{x}_2/2; \mathbf{p}_1, \mathbf{p}_2). \end{aligned} \quad (14)$$

We insert Eq. (13) into the expression for the two-particle probability, Eq. (6), perform the integration over  $k_i^0$  and obtain

$$\begin{aligned} \Pi(\mathbf{p}_1, \mathbf{p}_2) = \int d^3\delta k_1 d^3\delta k_2 d^3R_1 d^3R_2 d^3k_1 d^3k_2 d^4x_1 d^4x_2 \bar{S}(x_1, E_1, \mathbf{k}_1) \bar{S}(x_2, E_{12} - E_1, \mathbf{k}_2) \\ \times f_2(\mathbf{k}_1, \mathbf{k}_2, \mathbf{R}_1, \mathbf{R}_2; \mathbf{p}_1, \mathbf{p}_2) e^{-i\delta\mathbf{k}_1 \cdot [\mathbf{x}_1 + \mathbf{k}_1(t_2 - t_1)/m - \mathbf{R}_1] - i\delta\mathbf{k}_2 \cdot (\mathbf{x}_2 - \mathbf{R}_2)} \\ = \int d^3R_1 d^3R_2 d^3k_1 d^3k_2 dt_1 dt_2 \bar{S}(t_1, \mathbf{R}_1 - (t_2 - t_1)\mathbf{k}_1/m, E_1, \mathbf{k}_1) \bar{S}(t_2, \mathbf{R}_2, E_{12} - E_1, \mathbf{k}_2) \\ \times f_2(\mathbf{k}_1, \mathbf{k}_2, \mathbf{R}_1, \mathbf{R}_2; \mathbf{p}_1, \mathbf{p}_2). \end{aligned} \quad (15)$$

If we had used a different "reasonable" formula for Eq. (12) or kept more terms in the expansion of  $E(\mathbf{k} + \delta\mathbf{k})$ , we would have obtained the same formula as Eq. (15) except that the partition of energy into the source at  $x_1$  and the source at  $x_2$  would have been different. These details are not important since they will be absorbed into the approximation of the next paragraph.

In order to make the formalism tractable, that is, depend only on  $S(\mathbf{x}, E, (\mathbf{k}_1 + \mathbf{k}_2)/2)$ , we now make the assumption that the product of the matrix elements  $\bar{S}_1 \cdot \bar{S}_2$  depends weakly on the partition of the four-momentum. In order for the particles to interact,  $x_1$  and  $x_2$  must be very close together. The function  $\bar{S}$  should then have the same momentum dependence at both points. If the momentum dependence is thermal, then the product of the Boltzmann distributions has no dependence on  $k_1 - k_2$ . Even for arbitrary momentum dependence, the product  $\bar{S}_1 \cdot \bar{S}_2$  has, to first order, no dependence on relative momentum. If we do not make the approximation of weak dependence on the partition of four-momentum, the formalism is intractable, unless we know quantum details of the emission matrix  $\bar{S}(k, x)$  for  $k^0 \neq E(\mathbf{k})$ .

Replacing both  $\mathbf{k}_1$  and  $\mathbf{k}_2$  with  $(\mathbf{k}_1 + \mathbf{k}_2)/2$  in Eq. (15) yields

$$\begin{aligned} \Pi(\mathbf{p}_1, \mathbf{p}_2) = & \int d^3R_1 d^3R_2 d^3k_1 d^3k_2 dt_1 dt_2 \tilde{S} \left[ t_1, \mathbf{R}_1 - \frac{(\mathbf{k}_1 + \mathbf{k}_2)(t_2 - t_1)}{(2m)}, E_{12}/2, (\mathbf{k}_1 + \mathbf{k}_2)/2 \right] \\ & \times \tilde{S}(t_2, \mathbf{R}_2, E_{12}/2, (\mathbf{k}_1 + \mathbf{k}_2)/2) f_2(\mathbf{k}_1, \mathbf{k}_2, \mathbf{R}_1, \mathbf{R}_2; \mathbf{p}_1, \mathbf{p}_2). \end{aligned} \quad (16)$$

Since the total momentum of the pair is conserved during the evolution towards their asymptotic momentum states, we can substitute  $\mathbf{k}_1 + \mathbf{k}_2 = \mathbf{p}_1 + \mathbf{p}_2 = \mathbf{P}$ . We obtain

$$\begin{aligned} \Pi(\mathbf{p}_1, \mathbf{p}_2) = & \int d^3R_1 d^3R_2 d^3k_1 d^3k_2 dt_1 dt_2 \tilde{S} \left[ t_1, \mathbf{R}_1 - \frac{\mathbf{P}(t_2 - t_1)}{(2m)}, E_{12}/2, \mathbf{P}/2 \right] \\ & \times \tilde{S}(t_2, \mathbf{R}_2, E_{12}/2, \mathbf{P}/2) f_2(\mathbf{k}_1, \mathbf{k}_2, \mathbf{R}_1, \mathbf{R}_2; \mathbf{p}_1, \mathbf{p}_2). \end{aligned} \quad (17)$$

The emission function  $S$  is evaluated at the four-momentum  $P = (E(\mathbf{P}), \mathbf{P})$ . In general, the zeroth component of this four-vector is not equal to  $E_{12}$ . However, as long as  $\mathbf{p}_1 - \mathbf{p}_2$  is small, this difference can be neglected. This approximation allows us now to replace the function  $\tilde{S}(x_i, P/2)$  with the single-particle emission probability  $g(P/2, x)$ , see Eq. (10). We can now calculate the two-particle probability in terms of single-particle probabilities. It is prudent to make the same approximations in the expression for the single-particle emission probabilities. Then the correlation function for noninteracting particles will remain at unity even when  $\mathbf{p}_1 - \mathbf{p}_2$  is not small.

Dividing the two-particle emission probability from Eq. (17) by the single-particle emission probabilities thus yields for the two-particle correlation function

$$C(\mathbf{P}, \mathbf{q}) = \frac{\int d^4x_1 d^4x_2 d^3k_1 d^3k_2 g(\mathbf{P}/2, x_1) g(\mathbf{P}/2, x_2) f_2(\mathbf{k}_1, \mathbf{k}_2, \mathbf{x}_1 + (\mathbf{P}/2m)(t_2 - t_1), \mathbf{x}_2; \mathbf{p}_1, \mathbf{p}_2)}{\int d^4x_1 d^3k_1 g(\mathbf{P}/2, x_1) f_1(\mathbf{k}_1, \mathbf{x}_1; \mathbf{p}_1) \int d^4x_2 d^3k_2 g(\mathbf{P}/2, x_2) f_1(\mathbf{k}_2, \mathbf{x}_2; \mathbf{p}_2)} \quad (18)$$

Using the definition of the Wigner decompositions, Eq. (14), and the fact that the two-particle wave function can be factored into the center-of-mass wave function multiplied by the relative wave function,

$$\Phi(\mathbf{x}_1, \mathbf{x}_2; \mathbf{p}_1, \mathbf{p}_2) = \exp[-i(\mathbf{p}_1 + \mathbf{p}_2) \cdot (\mathbf{x}_1 + \mathbf{x}_2)/2] \phi((\mathbf{p}_1 - \mathbf{p}_2)/2, \mathbf{x}_1 - \mathbf{x}_2), \quad (19)$$

one finds for the integrals over the Wigner functions  $f_1$  and  $f_2$

$$\int d^3k_i f_1(\mathbf{k}_i, \mathbf{x}_i; \mathbf{p}) = 1, \quad (20)$$

$$\begin{aligned} \int d^3k_1 d^3k_2 f_2(\mathbf{k}_1, \mathbf{k}_2, \mathbf{x}_1, \mathbf{x}_2; \mathbf{p}_1, \mathbf{p}_2) &= \int d^3(k_1 + k_2) d^3 \left[ \frac{k_1 - k_2}{2} \right] f_2(\mathbf{k}_1, \mathbf{k}_2, \mathbf{x}_1, \mathbf{x}_2; \mathbf{p}_1, \mathbf{p}_2) \\ &= \int d^3(k_1 + k_2) d^3 \left[ \frac{k_1 - k_2}{2} \right] \delta^3(\mathbf{P} - \mathbf{k}_1 - \mathbf{k}_2) \\ &\quad \times \int d^3\delta r \exp[i\delta r \cdot (\mathbf{k}_1 - \mathbf{k}_2)/2] \phi^*(\mathbf{q}, \mathbf{x}_1 - \mathbf{x}_2 + \delta r/2) \phi(\mathbf{q}, \mathbf{x}_1 - \mathbf{x}_2 - \delta r/2) \\ &= |\phi(\mathbf{q}, \mathbf{x}_2 - \mathbf{x}_1)|^2. \end{aligned} \quad (21)$$

Inserting these relations into Eq. (18) now yields our final result, which was already given in Eq. (1).

The central assumption underlying our derivation is the approximation  $\tilde{S}(x, E, \mathbf{k}_i) \approx \tilde{S}(x, E, (\mathbf{k}_1 + \mathbf{k}_2)/2)$ . This approximation becomes exact when the emission function  $\tilde{S}(x, k)$  is broad, i.e., when its characteristic momentum is much larger than the relative momentum or the momentum spread of the resonance. In intermediate-energy heavy-ion collisions this is an appropriate assumption since the characteristic momenta are of the order of magnitude of a few hundred MeV/c and the relative momenta of interest are smaller than 50 MeV/c. (The important momentum components for the  ${}^2\text{He}$  "resonance" lie below 100 MeV/c.) If we keep the momentum dependence in Eq. (15), expanding  $\mathbf{k}_i$  about  $\mathbf{P}/2$ , we can show that this dependence cancels out in first order. Thus we expect the formalism to give very close to the correct answer, unless the characteristic momentum of the emission becomes quite small. Our derivation does not rely on the assumption that the system be semiclassical and that the thermal wavelength be much shorter than the

size of bound states or even the size of the emitting system. Our result is valid as long as the product of  $\tilde{S}_1 \cdot \tilde{S}_2$  depends only on  $\mathbf{k}_1 + \mathbf{k}_2$  and not  $\mathbf{k}_1 - \mathbf{k}_2$ . For systems which sample many states, such as a thermal system, this is a good assumption. Since usually there is no knowledge of the matrix elements as a function of  $k^0$ , these approximations are the best we can do. Fortunately, since we are interested in correlations for small relative momenta and since the characteristic momenta of the protons are sufficiently high, these are excellent approximations.

The correlation function  $C(\mathbf{P}, \mathbf{q})$  depends only on the final relative positions of all the particles with momentum  $\mathbf{P}/2$ . To make this clearer, we write Eq. (1) as

$$C(\mathbf{P}, \mathbf{q}) = \int d^3r F_P(\mathbf{r}) |\phi(\mathbf{q}, \mathbf{r})|^2, \quad (22)$$

where  $\mathbf{r} = \mathbf{r}_1 - \mathbf{r}_2$  is the relative coordinate of the emitted particles. The function  $F_P(\mathbf{r})$  is defined by

$$F_P(\mathbf{r}) = \frac{\int d^3R f(\mathbf{P}/2, \mathbf{R} + \mathbf{r}/2, t_>) f(\mathbf{P}/2, \mathbf{R} - \mathbf{r}/2, t_>)}{|\int d^3r' f(\mathbf{P}/2, \mathbf{r}', t_>)|^2} \quad (23)$$

where  $\mathbf{R} = \frac{1}{2}(\mathbf{r}_1 + \mathbf{r}_2)$  is the center-of-mass coordinate of the two particles. The Wigner function  $f(\mathbf{p}, \mathbf{r}, t_>)$  is the phase-space distribution of particles of momentum  $\mathbf{p}$  at position  $\mathbf{r}$  at some time  $t_>$  after both particles have been emitted:

$$f(\mathbf{p}, \mathbf{r}, t_>) = \int_{-\infty}^{t_>} dt g(\mathbf{p}, \mathbf{r} - \mathbf{p}(t_> - t)/m, t). \quad (24)$$

For a given momentum  $\mathbf{P}$ , the correlation has three degrees of freedom  $\mathbf{q}$ , which are a function of  $F_{\mathbf{p}}(\mathbf{r})$ . The most we can hope to extract from the correlation function is  $F_{\mathbf{p}}(\mathbf{r})$ , the normalized probability of two protons with the same momentum  $\mathbf{P}/2$  being separated by  $\mathbf{r}$ . We have shown in the derivation above that the calculation of  $F_{\mathbf{p}}(\mathbf{r})$  requires only the knowledge of the final phase-space distributions or the emission probability  $g(\mathbf{p}, \mathbf{r}, t)$ .

### III. DISCUSSION AND ILLUSTRATIVE CALCULATIONS

In this section, we will discuss the physical information contained in two-particle correlation functions, such as the source size and lifetime, and point out characteristic signatures of slowly cooling and exploding sources, respectively. The function  $F_{\mathbf{p}}(\mathbf{r})$ , Eq. (23), contains significant information about the dynamics of the collision. For instance, a long-lived source will lead to an extended separation when  $\mathbf{r}$  is parallel to the velocity  $\mathbf{P}/2m$ . Thus in addition to the spatial extent of  $F_{\mathbf{p}}(\mathbf{r})$  one gains insight into the lifetime of the collision.<sup>14</sup>

The  $\mathbf{P}$  dependence yields insight into the dynamics of the collision. Both the spatial size and the lifetime can depend on the total momentum. Cooling<sup>14,25,26</sup> is signified by increasingly large lifetimes for particles with smaller energies. We discuss this later in the section on the compound nucleus. Collective explosive flow is signaled by short lifetimes and shrinking apparent source dimensions for increasing energy.<sup>27</sup> There should be a transition in reaction mechanisms, from evaporative to exploding, at excitation energies near the nuclear binding energy. This is the dynamical equivalent of the liquid-gas phase transition. At low excitation, the nuclear matter slowly evaporates particles, cooling like a hot liquid drop. At sufficiently high excitation, nuclear matter explodes and expands to fill the available volume, like a gas. This is also discussed in Ref. 14.

The relative wave function  $\phi(\mathbf{q}, \mathbf{r})$  is influenced by three different effects: identical particle interference, short-range hadronic interaction, and the Coulomb repulsion of the protons. We briefly discuss how these three effects contribute to the correlation function and how the resulting correlation can be used to determine  $F_{\mathbf{p}}(\mathbf{r})$ .

To calculate the relative wave function numerically, we solved the Schrödinger equation for the  $l=0$  and  $l=1$  partial waves. For the relative wave function  $\phi(\mathbf{q}, \mathbf{r})$  we used the full solution Coulomb waves,<sup>28</sup>  $\phi_C(\mathbf{q}, \mathbf{r})$ , and added the modification  $\delta\phi(\mathbf{q}, \mathbf{r})$ , which is the contribution to the relative wave function from the first two partial waves minus the contribution which would have occurred if the strong interaction were absent. The Schrödinger equation was solved with the Reid soft-core potential.<sup>29</sup>

For identical noninteracting particles, the squared

wave function has the form  $|\phi(\mathbf{q}, \mathbf{r})|^2 \propto [1 \pm \cos(2\mathbf{q} \cdot \mathbf{r})]$ . In that case, the inverse Fourier transform of the correlation function would yield the complete three-dimensional function  $F_{\mathbf{p}}(\mathbf{r})$ . For spin-half particles, the correlation function is reduced to one-half at  $|\mathbf{q}|=0$  and returns to unity with a width of  $q_x \approx 1/R_x$ . Experiments that gate on the direction of the relative momentum can then determine all three spatial dimensions of  $F_{\mathbf{p}}(\mathbf{r})$ .

Coulomb interactions yield a dip in the correlation function which goes to zero as  $\mathbf{q}$  approaches zero. As long as the characteristic dimensions of  $F_{\mathbf{p}}(\mathbf{r})$  are much smaller than the two-proton Bohr radius of 58 fm, the shape of the dip does not depend on the shape or size of the source but only on the Gamov factor. For larger sources, the Coulomb interaction, too, provides information about both the source size and, to a weak degree, on the shape. The Coulomb dip in the correlation function at  $|\mathbf{q}|=0$  will diminish for large sources. The most unfortunate aspect of the Coulomb interaction is that the Coulomb dip lessens the number of available pairs at small relative momentum, making it more difficult to see the effects of identical particle interference.

Strong interactions provide excellent gauges of the size of smaller sources,  $R \lesssim 10$  fm. The  ${}^2\text{He}$  "resonance" appears as a bump in the proton-proton correlation function at a relative momentum of 20 MeV/c. (Strictly speaking, the  ${}^2\text{He}$  "resonance" is not a resonance, since the phase shift does not increase by  $90^\circ$ , but only by about  $60^\circ$ .) The size of the bump is proportional to the percentage of pairs whose relative position is within the size of the nearly bound state. Thus the height goes roughly as  $R^{-3}$ . This provides a very sensitive test of the size, but not of the shape.

For typical source sizes of about 5 fm, all three effects are important. Choosing a distribution  $F_{\mathbf{p}}(\mathbf{r})$  that fits the correlation function requires more than just the appropriate size as measured by a single parameter. One must have  $F_{\mathbf{p}}(\mathbf{r})$  correct for large  $\mathbf{r}$  in order to fit the correlation function at low  $\mathbf{k}$  in the Coulomb dip and one must have  $F_{\mathbf{p}}(\mathbf{r})$  correct at small  $\mathbf{r}$  in order to fit the height of the correlation function. If the source is not so large that the Coulomb dip erases the effect of identical particle interference, the shape must be chosen correctly as well to fit the correlation function for different directions of  $\mathbf{q}$ . Thus all the physical characteristics of  $F_{\mathbf{p}}(\mathbf{r})$  can be thoroughly tested with correlation measurements. In the following subsections we illustrate some of these qualitative expectations by calculations performed for simple analytical emission sources.

#### A. Spherical sources of negligible lifetime

The relative importance of antisymmetrization and the nuclear and Coulomb interactions depends on the size of the emitting system. In order to provide a quantitative comparison of these effects, we have calculated two-proton correlation functions for Gaussian sources of negligible lifetime,

$$g(\mathbf{p}, \mathbf{r}, t) = \rho(r)\delta(t - t_0) \\ = \rho_0 \exp(-r^2/r_0^2)\delta(t - t_0), \quad (25)$$

in which the nuclear interaction and the Pauli principle were turned off successively. These calculations are compared in Fig. 1 for a number of representative radius parameters ( $r_0=2.5, 5, 10,$  and  $20$  fm). The solid curves show the results of the full calculations which include the nuclear and Coulomb interactions and the Pauli exclusion principle. The dotted lines show calculations for which the nuclear interaction has been turned off; these calculations still include quantum effects of the two-proton Coulomb interaction and the antisymmetrization of the relative wave function. The dashed curves represent calculations for which both the nuclear interaction and the antisymmetrization of the relative wave function have been turned off. (These latter calculations differ from classical Coulomb trajectory calculations<sup>17</sup> since the Coulomb repulsion between the two protons is treated quantum mechanically. For large source dimensions or emission from long-lived sources, this difference should be of minor importance.) For radius parameters,  $r_0 \lesssim 10$  fm, both the antisymmetrization of the relative wave function and the nuclear interaction have important effects on the detailed shape of the calculated correlation functions. For much larger source dimensions,  $r_0 \gtrsim 20$  fm, the Coulomb interaction dominates and the neglect of the Pauli principle and the nuclear interaction can be justified.<sup>17</sup>

Most analyses of fast-particle-emission processes<sup>3-5, 10-13, 15-18</sup> have used sources of negligible lifetime with spherically symmetric Gaussian density distributions, Eq. (25). For spherically symmetric sources, the shape of the two-proton correlation function is rather insensitive to details of the density profile. To illustrate this point, we compare the shapes of two-proton correlation functions calculated for sources of negligible lifetime with Gaussian, Eq. (25), and uniform sharp-sphere density distributions,

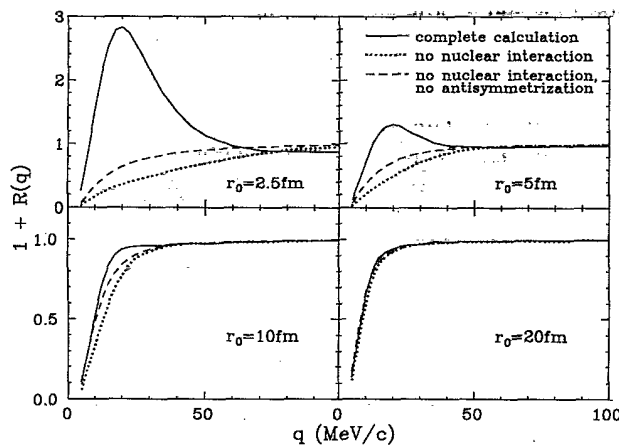


FIG. 1. Two-proton correlation functions calculated for short-lived Gaussian sources of representative radius parameters,  $r_0=2.5, 5, 10,$  and  $20$  fm. The solid curves show the result of the full calculations; the dotted curves show calculations for which the nuclear interaction is neglected; the dashed curves show calculations for which the nuclear interaction and the Pauli principle are neglected.

$$g(\mathbf{p}, \mathbf{r}, t) = \rho_s(r) \delta(t - t_0) \\ = \rho_0 \Theta(r) \Theta(R_s - r) \delta(t - t_0). \quad (26)$$

In Eq. (26),  $R_s$  is the sharp-sphere radius and  $\Theta(x)$  is the unit step function which vanishes for negative arguments. The solid and dotted curves in Fig. 2 represent calculations performed with Eqs. (25) and (26), respectively. In these calculations, the radius parameters have been adjusted to match the magnitudes of the maxima at  $q \approx 20$  MeV/c. The correlation functions calculated for these rather different density profiles are virtually identical in shape. Previously, Gaussian source parameters  $r_0$  have been translated<sup>1</sup> into equivalent sharp-sphere radii  $R_s$  by employing the approximate relation  $R_s \approx (\frac{5}{2})^{1/2} r_0$ . This relation can be justified by equating the rms radii of the two density distributions. Equivalent radii,  $r_0$  and  $R_s$ , of the two density profiles can also be defined by the requirement that the calculated correlation functions have maxima of identical height. Such equivalent radii are indicated by crosses in Fig. 3. These equivalent radii can be rather well described by the relation  $R_s = 1.493r_0 + 0.0475$  fm; this relation is represented by the solid curve in Fig. 3. For comparison, the analytically derived relation  $R_s = (\frac{5}{2})^{1/2} r_0$  is indicated by the dotted curve; it is a surprisingly good approximation.

### B. Spherical sources of finite lifetime

In order to illustrate the sensitivity of the shapes of two-proton correlation functions to the decay time of the emitting system, we have performed calculations under the simplifying assumption that particles are emitted from a spherical volume of radius  $R_s$  according to a simple exponential law,

$$g(\mathbf{p}, \mathbf{r}, t) \propto \rho_0 \Theta(r) \Theta(R_s - r) \Theta(t) p e^{-p^2/2mT - t/\tau}, \quad (27)$$

where  $T$  and  $\tau$  denote the (constant) source temperature and lifetime, respectively.

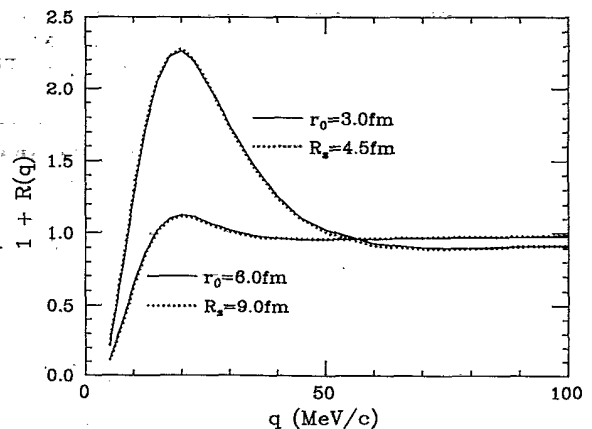


FIG. 2. Two-proton correlation functions calculated for sources of negligible lifetime assuming Gaussian (solid lines) and sharp-sphere (dotted lines) density distributions. The radius parameters  $r_0$  and  $R_s$  are indicated.

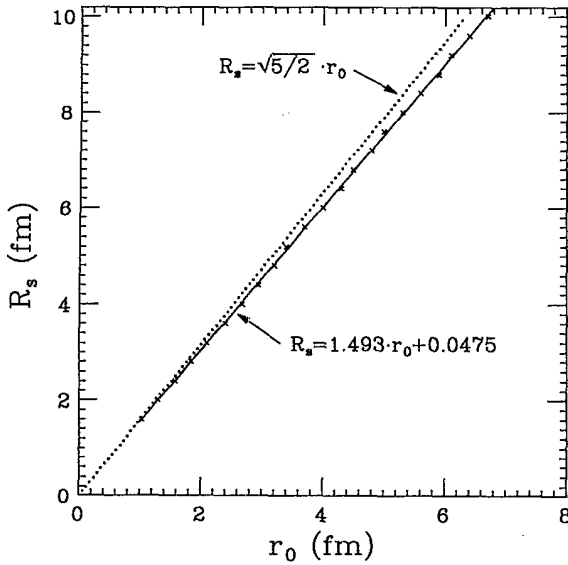


FIG. 3. Relation between radius parameters  $r_0$  and  $R_s$  of Gaussian and sharp-sphere density distributions for which equivalent two-proton correlation functions are obtained in the limit of negligible lifetime. Crosses indicate results of numerical calculations, the solid line represents a linear fit, and the dotted curve shows the relation  $R_s = (5/2)^{1/2} r_0$  used in the literature (Ref. 1).

Calculations for two-proton correlation functions, integrated over all relative orientations between  $\mathbf{P}$  and  $\mathbf{q}$ , are shown in Fig. 4. The parameters used in these calculations are given in the figure. The upper panel of the figure illustrates the sensitivity to the lifetime of the emit-

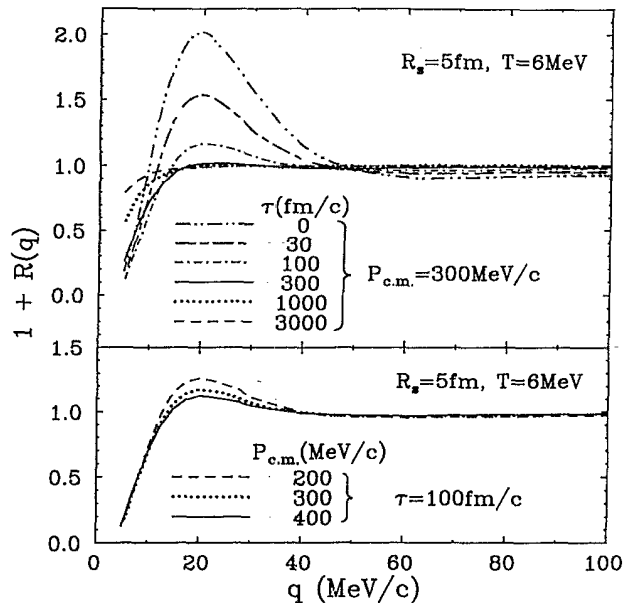


FIG. 4. Two-proton correlation functions predicted for emission from spherical sources of radius  $R_s = 5$  fm, decaying isotropically with fixed lifetime, Eq. (27). The top and bottom panels depict the dependence on lifetime  $\tau$  and total momentum  $P_{c.m.}$ , respectively.

ting system for proton pairs of total momentum,  $P_{c.m.} = 300$  MeV/c, measured in the rest frame of the emitting source. The calculated two-proton correlation functions exhibit considerable sensitivity to lifetimes of the order of 30–3000 fm/c. For much shorter lifetimes, the shape of the correlation function becomes dominated by the spatial dimension of the emitting system; for much longer lifetimes, the correlations disappear. The lower panel of Fig. 4 illustrates how the correlation function depends on the total momentum of the emitted proton pairs for the case of a fixed lifetime,  $\tau = 100$  fm/c. The calculated correlations become more pronounced for smaller total momenta, i.e., for particles emitted with lower kinetic energies. This dependence can be understood in terms of the spatial extent of the Wigner distribution. The longitudinal dimension of the apparent source is of the order of  $(P_{c.m.}/2m_p)\tau$ , where  $m_p$  denotes the proton mass. For fixed lifetime  $\tau$ , this quantity increases for larger values of  $P_{c.m.}$  and the correlation function becomes attenuated. Such a momentum dependence stands in contrast to experimental observations<sup>4,10–13,16,23,24</sup> and is opposite to that calculated for emission from compound nuclei for which the effects of cooling produce a strong momentum dependence of the effective decay times, see also the discussion in Sec. VII.

Figure 5 illustrates the dependence of the two-particle correlation function on the angle,  $\Psi = \cos^{-1}(\mathbf{P} \cdot \mathbf{q}/Pq)$ , between the relative and total momentum vectors of the two-proton pair. As was done in the experimental analysis of Ref. 24, we define longitudinal and transverse correlation functions by the cuts  $|\cos\Psi| \geq 0.77$  ( $\Psi = 0^\circ - 40^\circ$  or  $140^\circ - 180^\circ$ ) and  $|\cos\Psi| \leq 0.5$  ( $\Psi = 60^\circ - 120^\circ$ ). Different panels of Fig. 5 show transverse and longitudinal correlation functions calculated for different lifetimes  $\tau = 0, 10, 30, 100, 300,$  and  $1000$  fm/c. In these calculations, the total momentum of the proton

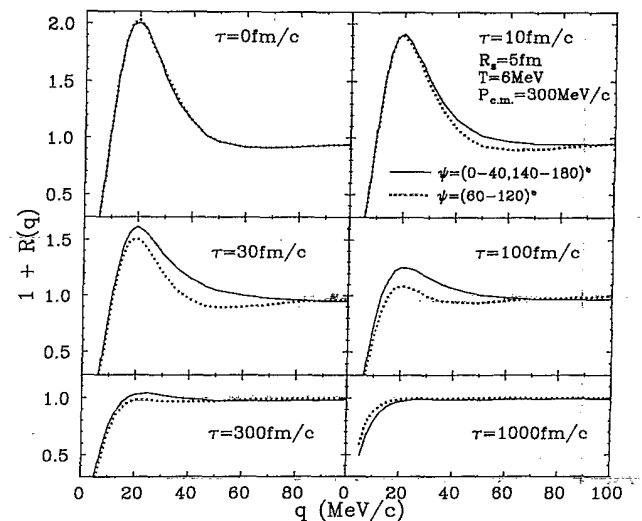


FIG. 5. Longitudinal and transverse correlation functions calculated for emission from sources decaying with constant lifetimes, Eq. (27). The parameters used in these calculations are indicated in the figure.

pair was kept constant at  $P_{c.m.} = 300$  MeV/c. For very short lifetimes,  $\tau \lesssim 10$  fm/c, the apparent source is essentially spherical in shape and lifetime effects are negligible for the calculation of the two-proton correlation function. For an intermediate time window,  $\tau \approx 30-300$  fm/c, longitudinal and transverse correlation functions are sensitive to the lifetime of the emitting system. For larger lifetimes,  $\tau \gtrsim 1000$  fm/c, this sensitivity is essentially lost as the average separation between emitted particles becomes so large that antisymmetrization effects become negligible. In fact, for extremely large lifetimes the effect is reversed because Coulomb-induced correlations contain a weak amount of directional information. The Coulomb force is parallel to the relative displacement of the protons; therefore, the Coulomb hole in the correlation function will be strongest when the relative momentum is parallel to the longest dimension of the pair's separation. For long-lived sources this is the longitudinal direction. Comparisons of longitudinal and transverse correlation functions yield the strongest information about the lifetime of the emitting system for lifetimes of the order of 30–300 fm/c. By more judicious choices of the gates on  $P_{c.m.}$ , one may stretch the sensitivity of such measurements beyond these rough boundaries.

#### IV. BUU TRANSPORT EQUATION FOR COLLISION DYNAMICS

In this section, we briefly review the derivation of the BUU transport equation which provides the basis for microscopic calculations for nonequilibrium particle emission in intermediate-energy nucleus-nucleus collisions. We start with the Schrödinger equation of the  $N$ -particle system,

$$i\partial_t \Psi = H\Psi. \quad (28)$$

Here,  $H$  is the  $N$ -particle Hamiltonian and  $\Psi$  is the  $N$ -particle wave function. From  $\Psi$ , one constructs the  $N$ -particle density,

$$\rho^{(N)} = \Psi\Psi^*, \quad (29)$$

which leads to the von Neumann equation of motion:

$$i\partial_t \rho^{(N)} = [H, \rho^{(N)}]. \quad (30)$$

We introduce the reduced density matrices via

$$\rho^{(n)}(\mathbf{r}_1, \dots, \mathbf{r}_n; \mathbf{r}'_1, \dots, \mathbf{r}'_n) = \frac{1}{(N-n)!} \int d^3r_{n+1} \dots d^3r_N d^3r'_{n+1} \dots d^3r'_N \rho^{(N)}(\mathbf{r}_1, \dots, \mathbf{r}_N; \mathbf{r}'_1, \dots, \mathbf{r}'_N). \quad (31)$$

Inserting Eq. (31) into Eq. (30) leads to the Bogoliubov-Born-Green-Kirkwood-Yvon (BBGKY) hierarchy of the reduced density matrices. This hierarchy links the time derivative of  $\rho^{(n)}$  to  $\rho^{(n+1)}$ . The lowest two members of the BBGKY hierarchy are

$$i\partial_t \rho^{(1)}(\mathbf{r}_1, \mathbf{r}'_1) = -\frac{1}{2m} (\nabla_{\mathbf{r}_1}^2 - \nabla_{\mathbf{r}'_1}^2) \rho^{(1)}(\mathbf{r}_1, \mathbf{r}'_1) + \int d^3r_2 [v(\mathbf{r}_1, \mathbf{r}_2) - v(\mathbf{r}'_1, \mathbf{r}_2)] \rho^{(2)}(\mathbf{r}_1, \mathbf{r}_2; \mathbf{r}'_1, \mathbf{r}_2) \quad (32)$$

and

$$i\partial_t \rho^{(2)}(\mathbf{r}_1, \mathbf{r}_2; \mathbf{r}'_1, \mathbf{r}'_2) = -\frac{1}{2m} \sum_{i=1}^2 (\nabla_{\mathbf{r}_i}^2 - \nabla_{\mathbf{r}'_i}^2) \rho^{(2)}(\mathbf{r}_1, \mathbf{r}_2; \mathbf{r}'_1, \mathbf{r}'_2) + [v(\mathbf{r}_1, \mathbf{r}_2) - v(\mathbf{r}'_1, \mathbf{r}'_2)] \rho^{(2)}(\mathbf{r}_1, \mathbf{r}_2; \mathbf{r}'_1, \mathbf{r}'_2) \\ + \sum_{i=1}^2 \int d^3r_3 [v(\mathbf{r}_i, \mathbf{r}_3) - v(\mathbf{r}'_i, \mathbf{r}_3)] \rho^{(3)}(\mathbf{r}_1, \mathbf{r}_2, \mathbf{r}_3; \mathbf{r}'_1, \mathbf{r}'_2, \mathbf{r}'_3). \quad (33)$$

A closed solution of the equations of the hierarchy is only possible if one truncates at a level  $n$  and with it neglects  $(n+1)$ -body correlations. Truncating at  $n=1$ , neglecting two-body correlations, and approximating  $\rho^{(2)}$  as an antisymmetrized product of one-body densities, one obtains the time-dependent Hartree-Fock (TDHF) equations:

$$i\partial_t \rho^{(1)} = [h, \rho^{(1)}], \quad (34)$$

where  $h$  is the single-particle Hamiltonian,

$$h(\mathbf{r}, \mathbf{r}') = -\delta^3(\mathbf{r} - \mathbf{r}') \frac{1}{2m} \nabla_{\mathbf{r}}^2 \\ + \delta^3(\mathbf{r} - \mathbf{r}') \int d^3r_2 \rho^{(1)}(\mathbf{r}; \mathbf{r}_2) v(\mathbf{r}, \mathbf{r}_2) \\ - \rho^{(1)}(\mathbf{r}, \mathbf{r}') v(\mathbf{r}, \mathbf{r}'). \quad (35)$$

Performing a Wigner transformation gives the Vlasov equation:

$$\partial_t f(\mathbf{p}, \mathbf{r}, t) + \frac{\mathbf{p}}{m} \cdot \nabla_{\mathbf{r}} f(\mathbf{p}, \mathbf{r}, t) \\ - \nabla_{\mathbf{r}} U(\mathbf{r}) \cdot \nabla_{\mathbf{p}} f(\mathbf{p}, \mathbf{r}, t) = 0. \quad (36)$$

In Eq. (36),  $U(\mathbf{r})$  is the mean-field or Hartree potential,

$$U(\mathbf{r}) = \int d^3r_2 v(\mathbf{r}, \mathbf{r}_2) \rho(\mathbf{r}, \mathbf{r}_2), \quad (37)$$

and  $f(\mathbf{p}, \mathbf{r}, t)$  is the Wigner transform of the single-particle density matrix,

$$f(\mathbf{p}, \mathbf{r}, t) = \int d^3s \rho^{(1)}(\mathbf{r} - \mathbf{s}/2, \mathbf{r} + \mathbf{s}/2) e^{i\mathbf{p} \cdot \mathbf{s}}. \quad (38)$$



In the derivation of Eq. (36), the semiclassical approximation has been used. This approximation is valid since typical wavelengths ( $\lambda \approx 2.5$  fm for  $p = 500$  MeV/c) are shorter than the size of the regions with the mean field (typically of the order of 8 fm diameter). The TDHF and Vlasov approximations to the many-body problem are

pure one-body theories in mean-field approximation in which all multiparticle correlations are neglected.

A truncation of the BBGKY hierarchy which includes two-body correlations, but neglects three- and higher-particle correlations leads to the Boltzmann-Uehling-Uhlenbeck (BUU) equation:

$$\begin{aligned} \partial_t f(\mathbf{p}, \mathbf{r}, t) + \frac{\mathbf{p}}{m} \cdot \nabla_r f(\mathbf{p}, \mathbf{r}, t) - \nabla_r U(\mathbf{r}) \cdot \nabla_p f(\mathbf{p}, \mathbf{r}, t) \\ = \frac{1}{2\pi^3 m^2} \int d^3 q'_1 d^3 q_2 d^3 q'_2 \delta \left[ \frac{1}{2m} (p^2 + q_2^2 - q_1'^2 - q_2'^2) \right] \delta^3(\mathbf{p} + \mathbf{q}_2 - \mathbf{q}'_1 - \mathbf{q}'_2) \frac{d\sigma}{d\Omega} \\ \times \{ \hat{f}(\mathbf{q}'_1, \mathbf{r}, t) \hat{f}(\mathbf{q}'_2, \mathbf{r}, t) [1 - \hat{f}(\mathbf{p}, \mathbf{r}, t)] [1 - \hat{f}(\mathbf{q}_2, \mathbf{r}, t)] \\ - \hat{f}(\mathbf{p}, \mathbf{r}, t) \hat{f}(\mathbf{q}_2, \mathbf{r}, t) [1 - \hat{f}(\mathbf{q}'_1, \mathbf{r}, t)] [1 - \hat{f}(\mathbf{q}'_2, \mathbf{r}, t)] \} . \end{aligned} \quad (39)$$

In Eq. (39),  $\hat{f}(\mathbf{p}, \mathbf{r}, t)$  is the phase-space density averaged over one phase-space cell. The left-hand side of the equation is the Vlasov term describing the temporal change of the one-body Wigner function  $f(\mathbf{p}, \mathbf{r}, t)$  due to the interaction of the nucleons with the mean field. The right-hand side is the collision integral which represents the effects of the correlations due to two-body collisions on the one-body Wigner function. Equation (39) was first obtained by Nordheim<sup>30</sup> as a quantum-mechanical extension of the Boltzmann equation which incorporates Fermion statistics.

and momenta of the pseudoparticles. The cell size for averaging was chosen to be  $\frac{1}{4}(\hbar/2\pi)^3$ .

## V. TWO-PROTON CORRELATION FUNCTIONS PREDICTED BY THE BUU EQUATION

Equation (39) is solved by using the pseudoparticle method.<sup>31</sup> In this method one compares the left-hand side of the equation to the complete differential of  $f$ :

Since the BUU equation is basically a theory describing the time evolution of the one-body phase-space distribution function, it seems at first sight surprising that it could be used to calculate two-particle correlation functions. Previously, it was shown<sup>32-36</sup> that the main features of two-proton coincidences at large angles are explained by the effects due to total momentum conservation, finite particle number, and/or collective motion in the reaction plane without requiring information about the detailed two-particle correlation function. However, within the formalism outlined in Sec. II, the knowledge of the one-body phase-space distribution function is sufficient for the calculation of the two-proton correlation function at small relative momenta and the characterization of the size and lifetime of the reaction zone formed in the nuclear collision.

$$\begin{aligned} \frac{d}{dt} f(\mathbf{p}, \mathbf{r}, t) = \frac{\partial}{\partial t} f(\mathbf{p}, \mathbf{r}, t) + \frac{d\mathbf{r}}{dt} \cdot \nabla_r f(\mathbf{p}, \mathbf{r}, t) \\ + \frac{d\mathbf{p}}{dt} \cdot \nabla_p f(\mathbf{p}, \mathbf{r}, t) . \end{aligned} \quad (40)$$

From Eqs. (39) and (40), one obtains a set of six coupled first-order differential equations for every occupied phase-space point:

$$\frac{dr_i}{dt} = \frac{p_i}{m} , \quad (41)$$

$$\frac{dp_i}{dt} = I_i(\mathbf{p}) - \frac{\partial}{\partial r_i} U(\mathbf{r}) . \quad (42)$$

Here,  $I_i(\mathbf{p})$  is the change in momentum  $p_i$  due to nucleon-nucleon collisions ( $i = 1, 2, 3$ ). The differential equations can be interpreted as the classical Hamiltonian equations of motion for a pseudoparticle. Since the total occupied phase space is proportional to the number of nucleons, it is convenient to specify the total number of phase-space points per nucleon as a measure for the numerical precision with which Eq. (39) is solved. In the present calculations, we have used up to 700 pseudoparticles per nucleon, resulting in a total of up to 172 200 coupled first-order differential equations which were solved simultaneously. The average phase-space occupancies used to determine the effects of the Pauli principle in the collision integral were determined from the coordinates

We solved the BUU equation by numerical methods which are similar to the ones introduced by Ref. 37, see also Ref. 38. The major new numerical technique used in our present calculations is the treatment of the Pauli exclusion principle. By explicitly storing  $\hat{f}(\mathbf{p}, \mathbf{r}, t)$  on a six-dimensional lattice in every time step, we were able to greatly speed up the computer program without relaxing the accuracy of the treatment of the Pauli-exclusion principle.<sup>39</sup> In our calculations of the correlation functions, appropriate averages over impact parameter, orientation of the reaction plane, and the indicated gates on the total momentum and the angle  $\Psi$  between the relative and total momentum of the two protons were taken into account.

In our "standard" calculations, the Wigner functions of emitted particles were constructed from nucleons emitted during a time interval following initial contact of the colliding nuclei of  $\Delta t_e = 140$  fm/c. Nucleons were considered as emitted when, during this time interval, the surrounding density fell below  $\rho_e = \rho_0/8$  and when subse-

quent interaction with the mean field did not cause recapture into regions of higher density. This test for recapture was continued over a time interval of  $\Delta t = 180$  fm/c after contact. The finite size of our lattice did not allow us to explore much larger emission times. However, the consideration of much larger emission times would not necessarily lead to more reliable results since, in our present approximation, the nuclei are not stable over long time scales and the BUU calculations become inaccurate due to spurious decays.

While our particular choice of the parameters  $\Delta t_e$  and  $\rho_e$  is reasonable, it involves a certain degree of arbitrariness. The sensitivity of the calculations to different choices of the emission time interval  $\Delta t_e$  and the freeze-out density  $\rho_e$  is illustrated in Fig. 6. Larger emission time intervals reduce the height of the maximum of the correlation function at  $q \approx 20$  MeV/c due to an increase of the average emission time. On the other hand, smaller freeze-out densities lead to a slight increase in the height of the maximum of the correlation function. This can be understood as follows: lower emission densities select subsets of particles considered as emitted for higher freeze-out densities by eliminating late emissions (i.e., particles which have not yet reached the lower densities) and thus selecting particles which had left the higher-density regime at earlier times. The corresponding reduction of the average temporal separation between emitted particles leads to enhanced correlations. Typically, different reasonable choices of  $\Delta t_e$  and  $\rho_e$  introduce

uncertainties of the order of 5–10% into the magnitude of the predicted correlation functions. However, in some instances these uncertainties can be larger.

The two major ingredients entering Eq. (39) are the mean-field potential  $U(r)$  and the nucleon-nucleon cross section  $d\sigma/d\Omega$ . In principle, one should be able to derive both from a fundamental nucleon-nucleon interaction, as has been done in some  $G$ -matrix calculations. In this paper, however, we proceed differently and use the conventional density-dependent Skyrme-type parametrization,

$$U(\rho) = A(\rho/\rho_0) + B(\rho/\rho_0)^\sigma, \quad (43)$$

where the parameters  $A$  and  $B$  are determined by the nuclear matter binding energy and the saturation density of nuclear matter at  $\rho = \rho_0$ . A choice of  $\sigma = 2$  results in  $A = -124$  MeV and  $B = 70.5$  MeV and a nuclear compressibility of  $K = 380$  MeV. This set of parameters is referred to as the “stiff” equation of state. The “soft” equation of state, with  $K = 200$  MeV, corresponds to the parameter set  $\sigma = \frac{7}{6}$ ,  $A = -356$  MeV, and  $B = 303$  MeV. The simple parametrization, Eq. (43), is only chosen to investigate the possible sensitivity of our calculations to the value of the nuclear compressibility.

We approximate the in-medium nucleon-nucleon cross section  $d\sigma/d\Omega$  by the energy-dependent free nucleon-nucleon cross section  $d\sigma_{NN}/d\Omega$  parametrized from experimental data. Since the exact value of the in-medium

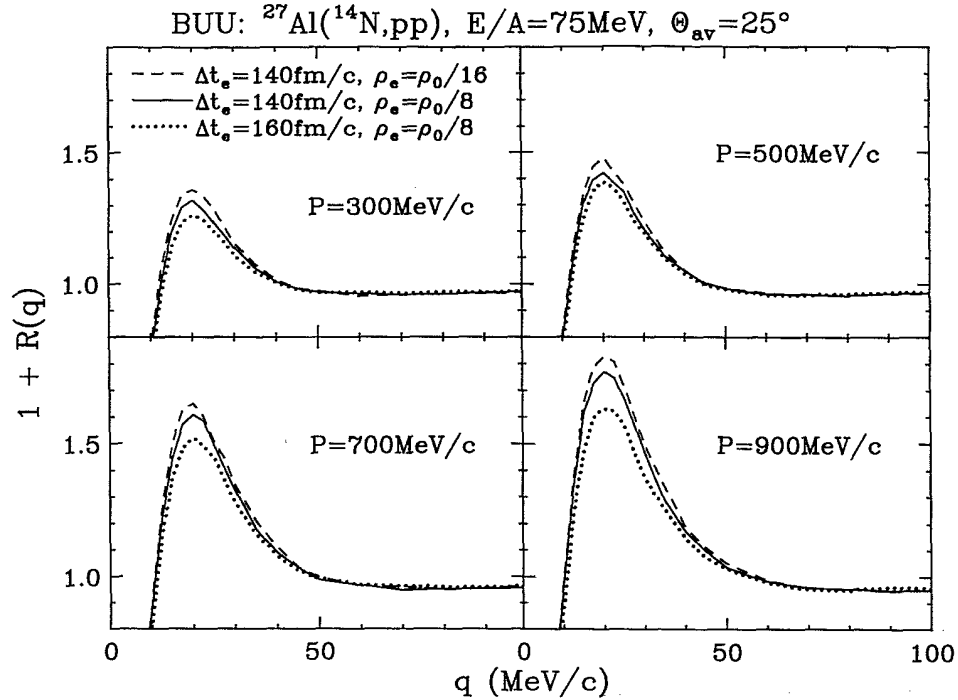


FIG. 6. Dependence of correlation functions predicted by BUU calculations on the emission time intervals  $\Delta t_e$  and the emission densities  $\rho_e$ . The values of individual parameter choices and selected total momenta of the proton pairs are given in the figure. In these calculations, the in-medium cross section was approximated by the experimental free nucleon-nucleon cross section, and the stiff equation of state was used.

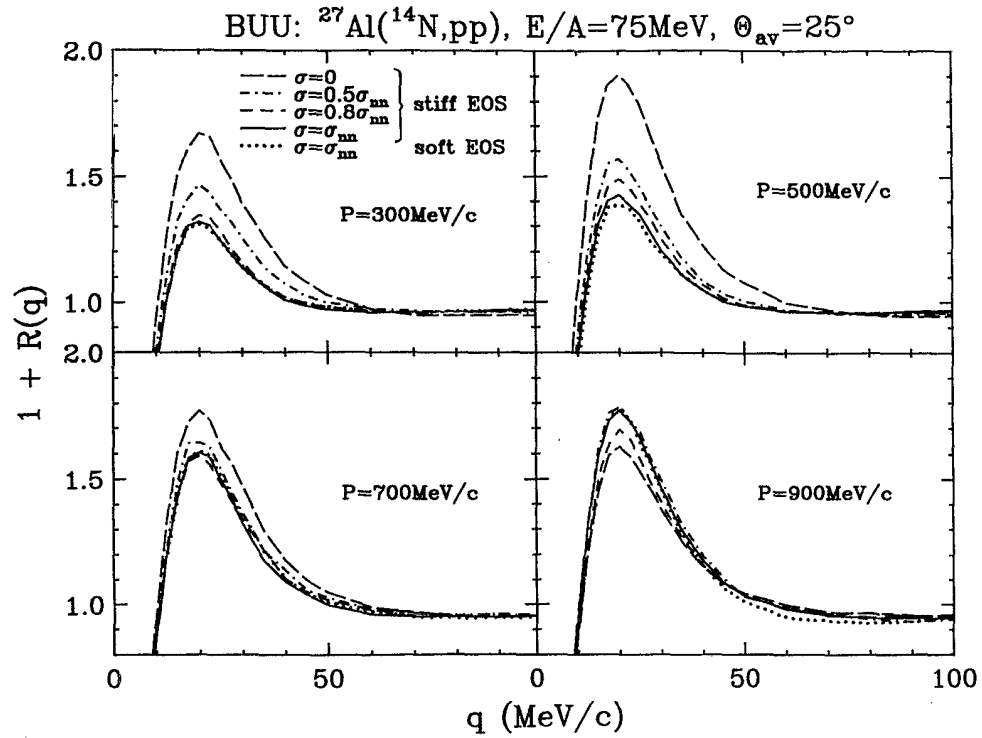


FIG. 7. Sensitivity of two-proton correlation functions to the nuclear equation of state (EOS) and the in-medium nucleon-nucleon cross section. Different panels show results calculated for different total momenta  $P$  of the proton pairs.

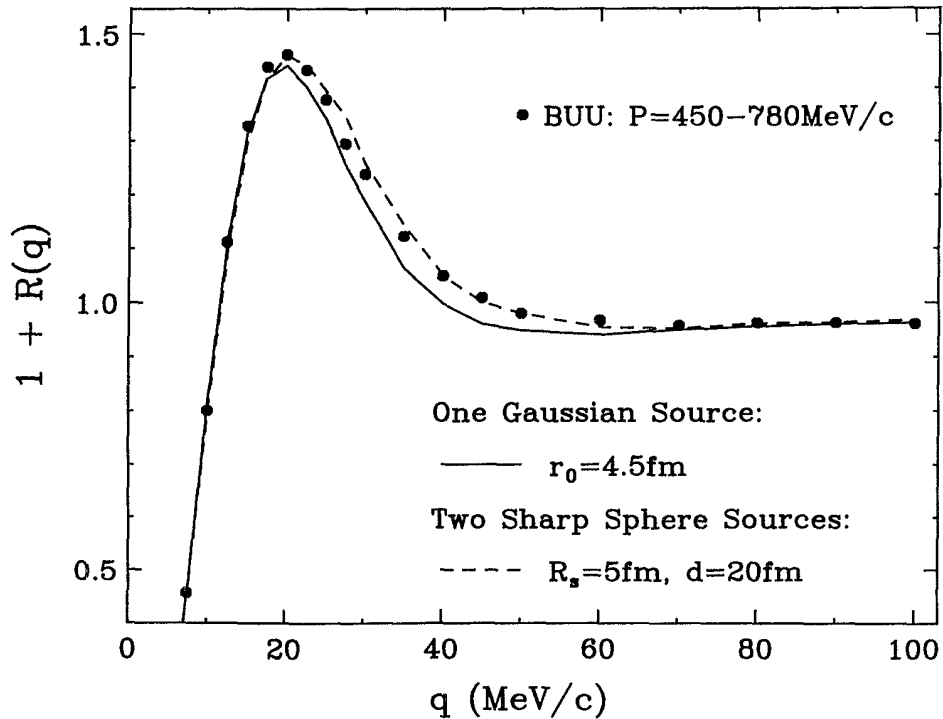


FIG. 8. Comparison of two-proton correlation functions predicted for different source geometries: The solid points represent the results of BUU calculations averaged over the momentum range  $P=450-780$  MeV/c. The curves show emission from sources of negligible lifetime: the solid and dashed curves are obtained, respectively, for a spherical Gaussian source of radius parameter,  $r_0=4.5$  fm, and a source consisting of two sharp spheres of radius  $R_s=5$  fm and separated by the distance  $d=20$  fm.

nucleon-nucleon cross section has attracted some recent attention, we also vary this input by multiplying the experimental  $d\sigma_{NN}/d\Omega$  by different factors ranging from 0 to 1.

For our numerical example, we calculate two-proton correlation functions for protons emitted at the laboratory angles  $\theta_{lab} \approx 25 \pm 9^\circ$  for  $^{14}\text{N} + ^{27}\text{Al}$  collisions at  $E/A = 75$  MeV, in close correspondence to the measurements of Ref. 24. Unless stated differently, we will use the stiff equation of state and in-medium cross sections equal to the experimental free nucleon-nucleon cross sections.

Figure 7 shows correlation functions calculated from Wigner functions predicted by the BUU equation using various assumptions on the in-medium nucleon-nucleon cross section and the stiffness of the equation of state. Individual panels of the figure show correlation functions calculated for different values of the total laboratory momenta  $P$  of the proton pairs. The solid and dotted curves show correlation functions predicted for the stiff and soft equations of state, using  $d\sigma/d\Omega = d\sigma_{NN}/d\Omega$ . These two calculations are very similar, indicating little sensitivity of the two-proton correlation functions to the stiffness of the equation of state. The solid, dashed, dot-dashed, and dot-dot-dashed curves represent calculations with the stiff equation of state performed with the assumption that the in-medium nucleon-nucleon cross section is equal to 1.0, 0.8, 0.5, and 0.0 times the free nucleon-nucleon cross section. For  $P \lesssim 700$  MeV/c, the predicted correlation functions become more pronounced for decreasing values of  $d\sigma/d\Omega$ , indicating that the space-time characteristics of the emitting system is more sensitive to the magnitude of the in-medium nucleon-nucleon cross section than to the stiffness of the equation of state.

Figure 8 compares the detailed shapes of two-proton correlation functions predicted for different space-time geometries. The solid points show correlation functions predicted from the BUU equation, averaged over the indicated range of total momenta  $P$  of the proton pairs. These calculations are in excellent agreement with existing data.<sup>24</sup> The solid curve shows results obtained for instantaneous emission from a Gaussian source, Eq. (25), with radius parameter  $r_0 = 4.5$  fm. The two-proton correlation function calculated for the Gaussian source exhibits a narrower maximum than that calculated for the more realistic density distribution obtained by means of the BUU equation. This difference in shape can be attributed to the fact that sources predicted by the BUU equation are nonspherical. To illustrate the sensitivity of the shape of two-proton correlation functions to the source geometry, we show the correlation function predicted for emission from a source consisting of two sharp spheres of negligible lifetime. Both spheres were assumed to have radii of  $R_s = 5$  fm, and the centers of the two spheres were assumed to be separated by a distance of  $d = 20$  fm and aligned along the beam direction. The correlation function for this two-source distribution is depicted by the dashed curve in Fig. 8; it has a wider maximum than the single Gaussian source distribution and is rather similar in shape to that predicted from the BUU calculations. (Remember that two-proton correlation

functions obtained for single spherical sources of sharp sphere and Gaussian density profiles are virtually indistinguishable in shape; see also the discussion of Figs. 2 and 3.)

Figures 9 and 10 depict the space-time evolution of the collision process as predicted by the BUU equation. Figure 9 shows the time evolution of the nucleon density in the reaction plane for a  $^{14}\text{N} + ^{27}\text{Al}$  collision at  $E/A = 75$  MeV and an impact parameter of 2 fm. Different panels of the figure represent snapshots taken at the indicated times after contact of the colliding nuclei. The calculations predict that the two colliding nuclei essentially survive the collision and separate into two hot nuclear objects, which may then decay on longer time scales for which BUU calculations cannot make accurate predictions. More relevant for the calculations of two-proton correlation functions is the density distribution of the em-

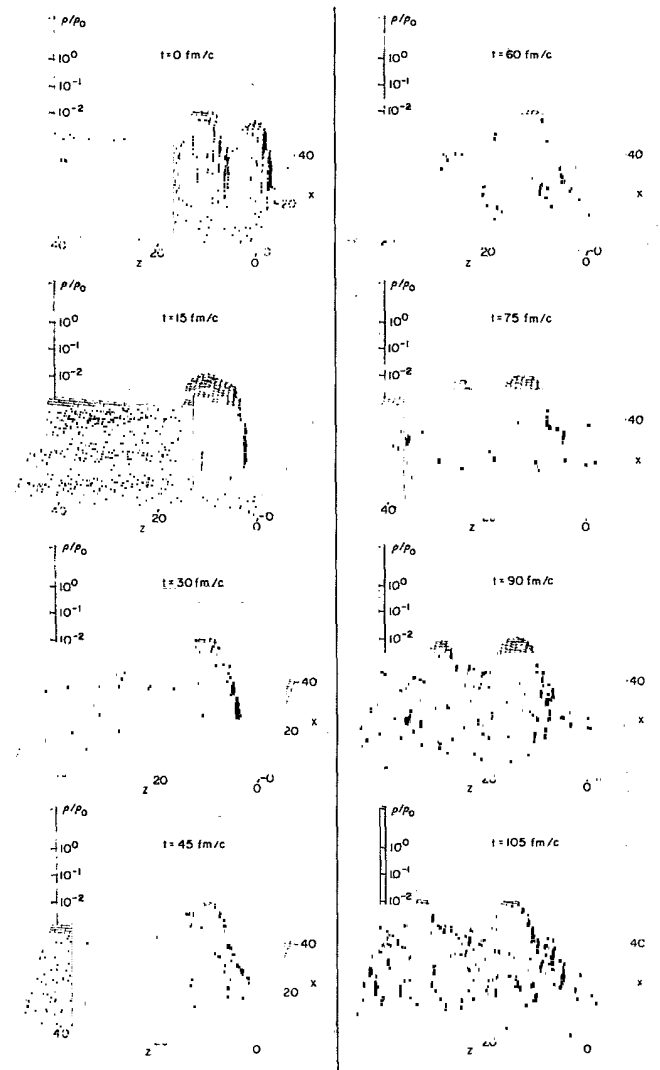


FIG. 9. Nucleon density distributions in the reaction plane calculated from the BUU equation for  $^{14}\text{N} + ^{27}\text{Al}$  collisions at  $E/A = 75$  MeV and for an impact parameter of  $b = 2$  fm. Different panels depict the distributions at different times  $t$ .

itted nucleons in the reaction plane, shown in Fig. 10 for selected times after the initial contact of the colliding partners. The distribution of emitted nucleons clearly undergoes an evolution from a near-spherical source at early times to a two-source distribution at larger times. This two-source distribution at larger times may explain the similarity of the correlation functions obtained for a two-sphere distribution with that predicted by the BUU calculations.

The nonspherical shapes of the Wigner functions predicted by the BUU calculations should be reflected in differences between longitudinal and transverse correlation functions. Longitudinal and transverse correlation functions predicted by BUU calculations are shown in Fig. 11. We have adopted the angular cuts,  $\Psi = \cos^{-1}(|\mathbf{P} \cdot \mathbf{q}|/|\mathbf{P}||\mathbf{q}|) = 0^\circ - 40^\circ$  and  $60^\circ - 90^\circ$ , for the calculation of longitudinal and transverse correlation functions, respectively. For the transverse correlation functions, we define the in-plane and out-of-plane directions by constraints on the azimuthal angle  $\phi$  of the relative momentum vector  $\mathbf{q}$  in a coordinate system with the  $z$  axis parallel to the total momentum vector  $\mathbf{P}$  of the pro-

ton pair. Defining  $\phi = 0^\circ$  as the plane spanned by the beam direction and  $\mathbf{P}$ , the in-plane transverse correlation function corresponds to the cut  $|\phi - n\pi| \leq 30^\circ$  ( $n = 0, 1, 2$ ); the out-of-plane transverse correlation functions corresponds to the cut  $|\phi - (2n + 1)\pi/2| \leq 30^\circ$  ( $n = 0, 1$ ). Different panels of the figure show the results for the indicated cuts on the total momenta of the proton pairs. In general, the out-of-plane transverse correlation functions are smaller than the in-plane transverse correlation functions since they are less affected by finite lifetime effects and collective velocity components. At low momenta, the longitudinal correlation function is more pronounced than the transverse correlation functions, possibly due to slow emission times; at higher momenta, longitudinal and in-plane transverse correlation functions are comparable in magnitude.

Details of the Wigner function must depend on the impact parameter of the collision. The predicted dependence is illustrated in Fig. 12; the various cuts on the total momentum of the proton pairs are indicated for the individual panels of the figure. In order to summarize the predicted trends, Fig. 13 shows the heights of the maxima

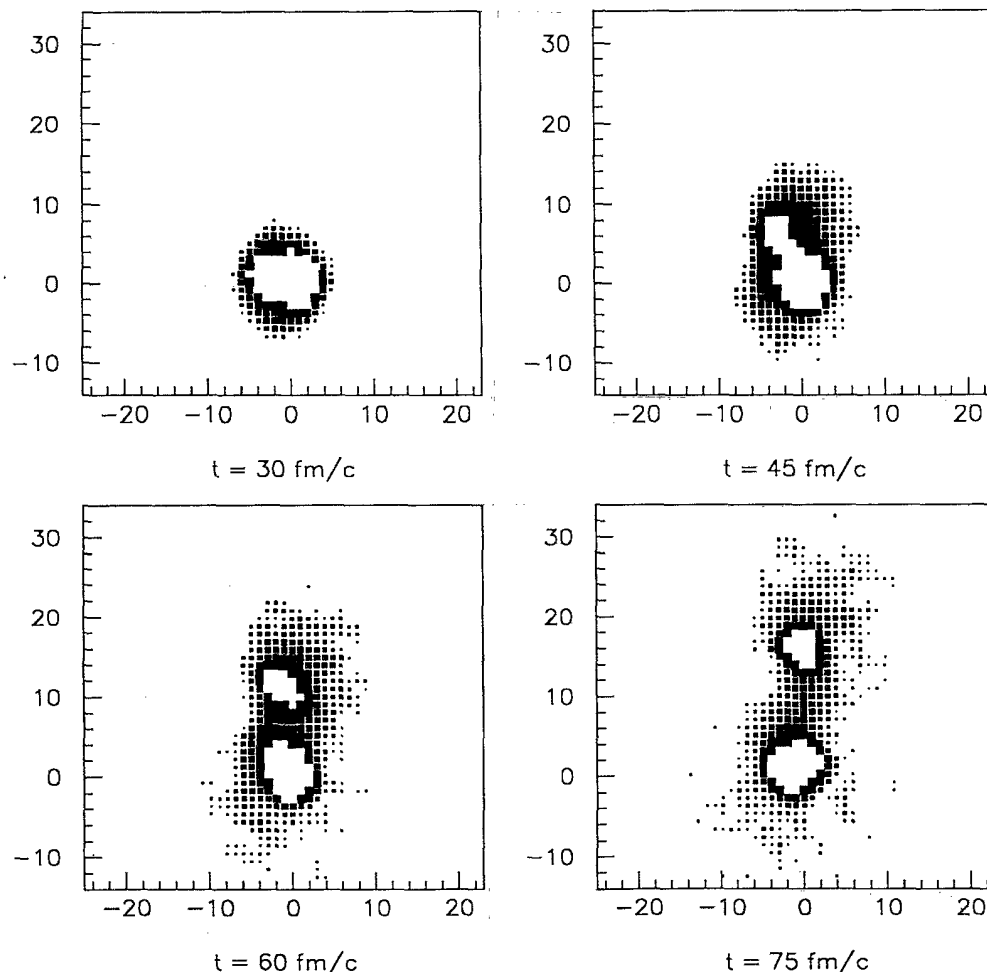


FIG. 10. Spatial distributions of emitted nucleons in the reaction plane calculated from the BUU equation for  $^{14}\text{N} + ^{27}\text{Al}$  collisions at  $E/A = 75 \text{ MeV}$  and for an impact parameter of  $b = 2 \text{ fm}$ . Different panels depict the distributions at different times  $t$ .

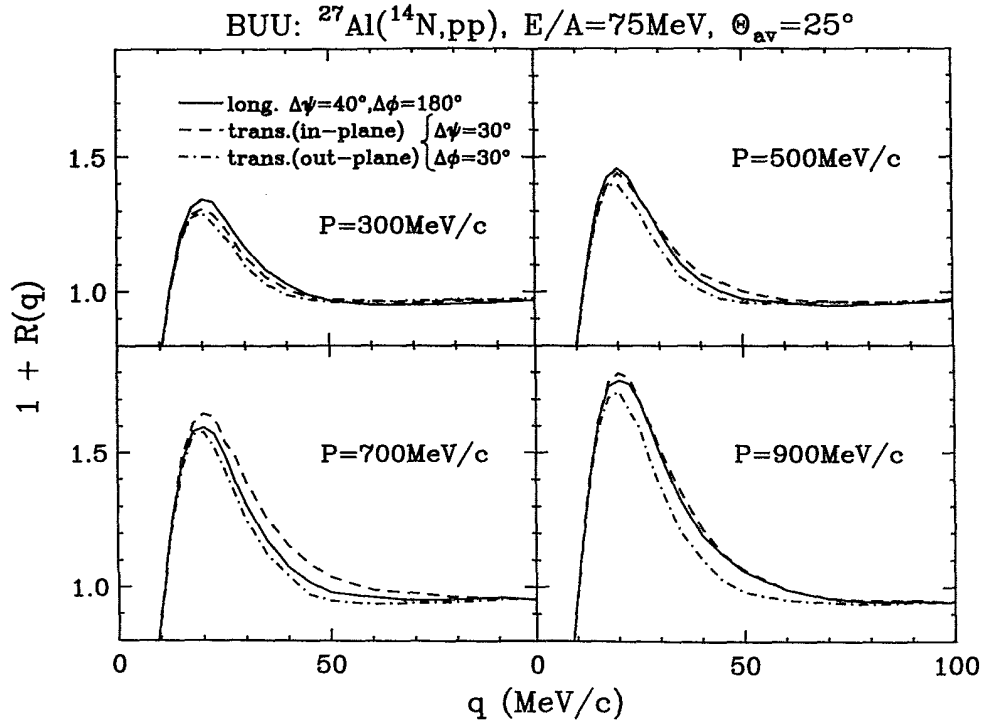


FIG. 11. Longitudinal and transverse correlation functions predicted by BUU calculations for  $^{14}\text{N}+^{27}\text{Al}$  collisions at  $E/A=75$  MeV for particle pairs for the indicated total momenta  $P$ .

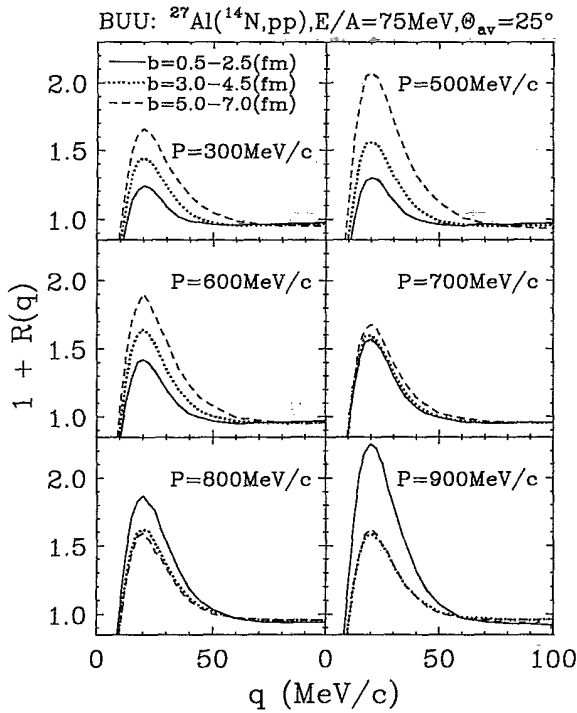


FIG. 12. Two-proton correlation functions predicted by BUU calculations for  $^{14}\text{N}+^{27}\text{Al}$  collisions at  $E/A=75$  MeV for the indicated impact parameters and total momenta of the emitted proton pairs.

of the calculated correlation functions as a function of  $P$  for different ranges of impact parameters.

For small impact parameters,  $b=0.5-2.5$  fm, the predicted correlation functions increase in magnitude as a function of increasing total momentum of the emitted particles, consistent with shorter time scales for the emission of more energetic particles.

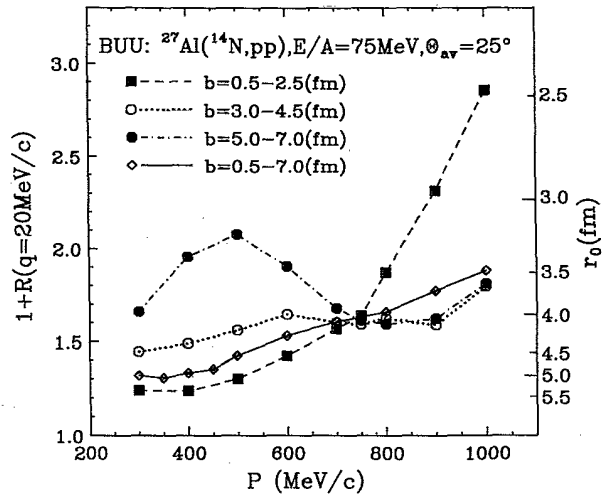


FIG. 13. Momentum dependence of the heights of the maxima of two-proton correlation functions predicted by BUU calculations for  $^{14}\text{N}+^{27}\text{Al}$  collisions at different impact parameters. Lines connect points corresponding to a given impact parameter to guide the eye.

For peripheral collisions,  $b=5-7$  fm, the calculated correlations are weakest for proton pairs with very high,  $P \approx 800$  MeV/c, or very low momenta,  $P \lesssim 300$  MeV/c; they are largest at intermediate momenta,  $P \approx 500$  MeV/c. This correlation pattern may be understood in terms of emission from fairly well defined projectilelike and targetlike sources. Proton pairs of low and high momenta correspond to low-energy emissions in the rest frames of targetlike and projectilelike sources, respectively. More energetic emissions from these sources are selected by intermediate momenta. For these emissions the correlation functions are expected to be enhanced because of the reduced size of the participant zone and/or because of shorter emission time scales. However, nucleon-nucleon collisions appear to play only a minor role since the maximum of the correlation function at  $P \approx 500$  MeV/c remains when the in-medium nucleon-nucleon cross section is set to zero.

For intermediate impact parameters,  $b \approx 3-4.5$  fm, the predicted momentum dependence is weak, most likely because of overlapping contributions from participant and spectator regions.

For total momenta,  $P \lesssim 700$  MeV/c, more pronounced correlations are observed for peripheral than for central collisions—in accordance with a simple geometric interpretation of the size of the reaction zone. However, for protons emitted with velocities higher than the beam velocity,  $P > 2p_{\text{beam}} \approx 760$  MeV/c, the maxima of the predicted correlation functions are larger for central than for peripheral collisions. Apparently, high-energy particles from central collisions are emitted on a very fast time scale. It may be speculated that such fast emission processes may be related to Fermi jets,<sup>40</sup> i.e., nucleons accelerated by the action of the mean field and emitted without significant nucleon-nucleon collisions. However, because of the semiclassical nucleonic momentum distribution used in our calculations, the predicted correlations may not be reliable for the highest momenta,  $P > 1000$  MeV/c, and should be viewed with caution. In any case, the calculations clearly indicate that one should be able to extract a wealth of information about the space-time evolution of the reaction zone by detailed investigations of the momentum and impact parameter dependence of two-proton correlation functions. Previous measurements of two-particle correlation functions did not determine the simultaneous dependence on impact parameter and momentum of the emitted particle pair and thus averaged over valuable information. New measurements capable of determining such dependences are clearly desirable.

## VI. EVAPORATIVE EMISSION

Correlation functions for particle evaporation from long-lived compound nuclei can be calculated by using the Wigner-function formalism<sup>14</sup> outlined in Sec. II. We have used the statistical model of Ref. 25 to construct Wigner functions for evaporative emission from equilibrated compound nuclei. In this model, the average particle emission is calculated from a generalized Weisskopf formula and cooling of the compound nucleus is calculat-

ed from the average mass and energy emission rates.<sup>25</sup>

This generalized Weisskopf formula<sup>25</sup> gives the probability per unit time and energy intervals of emitting a particle  $b$  with energy  $E$  at time  $t$  from a compound nucleus  $c$ :

$$\frac{d^2 N_b}{dE dt} = (2S_b + 1) \left[ \frac{m_b \pi R_b^2}{\pi^2 \hbar^3} \right] (E - V_b) \Theta(E - V_b) \times \exp \left[ \frac{-E + Z_b F(T, \rho_\pi) + N_b F(T, \rho_\nu) - B_b}{T} \right]. \quad (44)$$

Here,  $S_b$ ,  $m_b$ ,  $Z_b$ ,  $N_b$ , and  $E$  denote the spin, mass, charge, neutron number, and energy of the emitted particle;  $T$  is the temperature of the compound nucleus;  $F(T, \rho_\pi)$  and  $F(T, \rho_\nu)$  are the Helmholtz free energies per particle for protons and neutrons, respectively, and  $\Theta(x)$  is the unit step function. The free energies were calculated by assuming that the nucleons behaved like an ideal Fermi gas with a density of  $\rho = 0.145$  fm<sup>-3</sup>. The height of the Coulomb barrier,  $V_b$ , was taken as the Coulomb energy between the daughter nucleus and the emitted fragment when they are separated by the absorption radius  $R_b$ . For simplicity, the absorption radius was calculated as

$$R_b = r_0 [(A_c - A_b)^{1/3} + A_b^{1/3}], \quad r_0 = 1.2 \text{ fm}. \quad (45)$$

Here,  $A_c$  and  $A_b$  denote the mass numbers of the parent nucleus  $c$  and the emitted particle  $b$ , respectively. The binding energy  $B_b$  is the difference in masses of the parent nucleus and that of the daughter nucleus and the emitted particle. The masses of parent and daughter nuclei were calculated from a liquid-drop formula:

$$M(A, Z)c^2 = Zm_p c^2 + (A - Z)m_n c^2 - [14.1 A - 13 A^{2/3} - 0.595 Z^2 A^{-1/3} - 19(A - 2Z)^2 / A] \text{ MeV}. \quad (46)$$

The spatial distribution of emission points was chosen to be uniform in the two coordinates transverse to the velocity of the emitted particles; the third coordinate was chosen such that the emission point corresponds to the surface of the sphere of radius  $R_b$ . For particles with energies very near the Coulomb barrier, this is not a particularly satisfying choice. These particles undergo a significant change in their trajectory due to the Coulomb field of the compound nucleus. Distortions of two-proton correlation functions by deflections of the emitted protons in the Coulomb field of the daughter nucleus are manifestations of long-range three-body effects. Such effects are not incorporated in the formalism presented in Sec. II. We also neglected effects due to angular momentum coupling which, for rapidly rotating compound nuclei, could modify the extracted radii by up to 20%.<sup>19</sup>

If the spatial separation between emitted protons is much larger than the two-proton Bohr radius of 58 fm, one cannot only neglect the identical-particle interference of the emitted protons and their strong mutual interac-

tion, but also the quantum nature of their mutual Coulomb repulsion. Under these conditions, one can calculate correlation functions from the classical Coulomb trajectories, where the electric field of both protons and that of the compound nucleus are taken into account.<sup>17</sup> For compound nuclei with excitation energies below about 2.0 MeV/nucleon, emission time scales are sufficiently large that the above conditions are satisfied; classical trajectory calculations should provide a good approximation.

For increasingly high excitation energies, the time scales for emission become shorter. As the protons are emitted close to one another, the quantum nature of the Coulomb interaction, identical-particle statistics, and the strong interaction become important in that order. Fortunately, Coulomb deflections in the field of the compound nucleus become less important for particles emitted with kinetic energies significantly above the Coulomb barrier. For collisions with sufficient energy to dissolve the nuclei,  $E/A \gtrsim 50$  MeV, the neglect of three-body effects for the two-proton relative wave function should provide a good approximation. At these energies, the effects of the strong interaction and identical-particle interactions dominate. These effects can only be calculated by a full quantum treatment of the relative wave function.

## VII. NUMERICAL CALCULATIONS

It is instructive to explore the sensitivity of the calculated correlation functions to various parameters and momentum cuts. The following illustrative calculations are performed for narrow ranges of the total momenta  $P_{c.m.}$  of the emitted particle pairs. (The momenta  $P_{c.m.}$  are defined with respect to the compound-nucleus rest frame.)

The shape of the two-proton correlation function depends on the time scale governing the emission of the detected particles. For particle emission from equilibrated compound nuclei, this time scale depends on the level density and, therefore, on the initial temperature. Because of cooling via particle emission, the time scale also depends on the energy of the emitted particles. In Figs. 14 and 15, such dependences are illustrated for the decay of highly excited  $^{156}\text{Ho}$  nuclei. Figure 14 shows the calculated time dependence of the respective emission processes, i.e., the relative probability per unit time for the emission of the specified protons. The predicted two-proton correlation functions are shown in Fig. 15. The top panels in the two figures present calculations for initial temperatures  $T = 5, 10,$  and  $20$  MeV, keeping the total momentum of the two-proton pair fixed at  $P_{c.m.} = 400 \pm 10$  MeV/c. (This momentum bin selects protons of kinetic energy  $E_{c.m.}/A \approx 21$  MeV in the compound-nucleus rest frame.) At low temperatures,  $T \lesssim 5$  MeV, the decay times are large and the predicted correlation functions exhibit only a minimum at  $q \approx 0$  MeV/c. With increasing temperature, the decay times decrease and the minimum at  $q = 0$  MeV/c becomes more pronounced. For very hot nuclear systems,  $T \gtrsim 20$  MeV, the calculated emission time scales become so short that

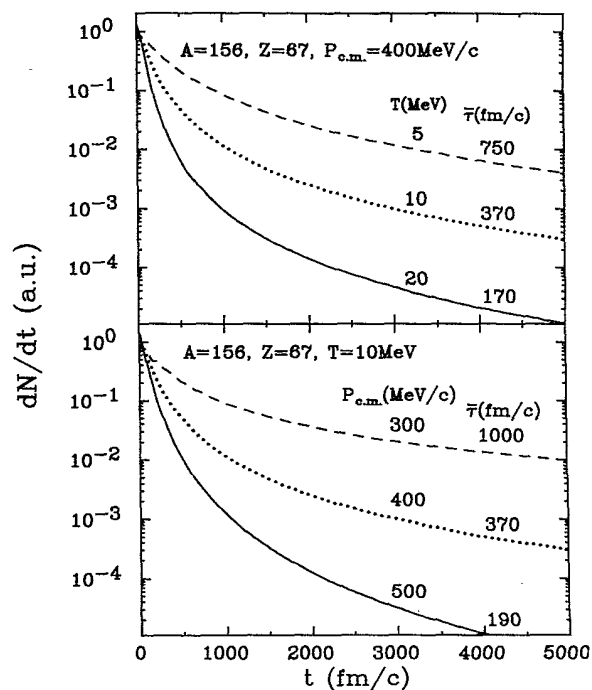


FIG. 14. Temporal evolution of particle emission from equilibrated  $^{156}\text{Ho}$  nuclei of different initial temperatures  $T$  (top panel) and for different total momenta  $P_{c.m.}$  (bottom panel) of the emitted two-proton pairs.

the two-proton nuclear interaction becomes significant and the maximum in the correlation function at  $q \approx 20$  MeV/c emerges. The bottom panels of Figs. 14 and 15 show calculations for different total momenta  $P_{c.m.}$  and fixed initial temperature  $T = 10$  MeV. Because of cooling of the compound nucleus, particles of higher energy are

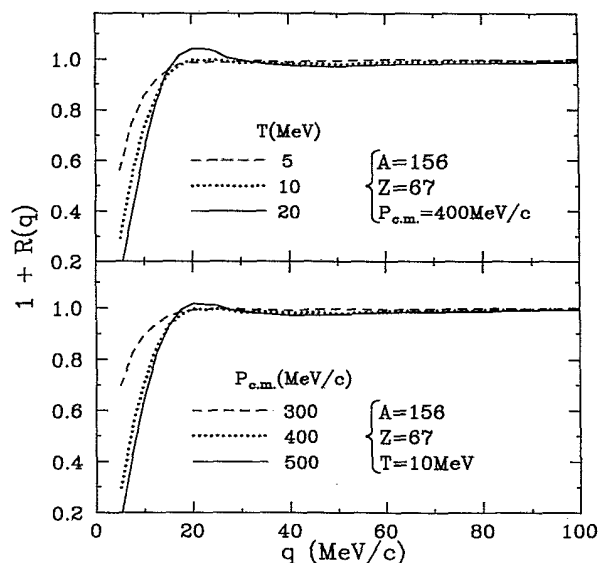


FIG. 15. Dependence of the two-proton correlation function on the initial temperature  $T$  (top panel), and on the total momentum  $P_{c.m.}$  (bottom panel) of emitted proton pairs calculated for the decay of equilibrated  $^{156}\text{Ho}$  nuclei.



emitted on faster time scales than particles of lower energy. As a consequence, the two-proton correlation functions reflect smaller apparent source dimensions for the emission of particles of increasing energy. At lower temperatures, qualitatively similar dependences exist, but their effects on the two-proton correlation functions are less visible due to the larger emission times.

For fixed excitation energy  $E^*$ , the decay rate of a compound nucleus depends on the relation between excited energy and temperature since higher temperatures lead to higher emission rates and, therefore, to smaller apparent source dimensions. Figure 16 illustrates the sensitivity of the calculated two-proton correlation functions to the assumed relation between excitation energy and temperature for the decay of  $^{156}\text{Ho}$  compound nuclei of fixed initial excitation energy,  $E^*/A=6.0$  MeV. In these calculations, the level density was taken as that of an ideal Fermi gas of the indicated spatial density  $\rho$ . For an ideal Fermi gas, the relation between excitation energy and temperature is given to first order by

$$T^2 = E^*/a. \quad (47)$$

The level density parameter  $a$  depends on the Fermi energy  $\epsilon_F$ :

$$a = \frac{\pi^2 A}{4\epsilon_F} \approx 0.065 A (\rho_0/\rho)^{2/3} \text{ MeV}^{-1}. \quad (48)$$

In Eq. (48), we have used the relation  $\epsilon_F \approx 38(\rho/\rho_0)^{2/3}$  MeV, where  $\rho_0 \approx 0.17 \text{ fm}^{-3}$  denotes the density of normal nuclear matter. For reference, the level density parameters are also indicated in Fig. 16. The calculations indi-

cate only a moderate sensitivity to the level density parameter. As expected, higher temperatures produce shorter emission times and, hence, more pronounced correlations.

Particle emission rates depend largely upon the temperature of the compound nucleus. Yet, the initial temperature does not specify the decay characteristics unambiguously, because different level density parameters represent different heat capacities of the decaying nuclear system. Figure 17 shows the sensitivity of the calculated two-proton correlation functions to the level density parameter for  $^{156}\text{Ho}$  compound nuclei of fixed initial temperature,  $T=10$  MeV. The predicted correlations are slightly more attenuated for larger level density parameters, i.e., for increasing values of the heat capacity of the compound nucleus. However, the sensitivity is not very pronounced; it is even less significant at lower temperatures.

Since the predicted emission times depend strongly on the momenta of the emitted particles, the differences between longitudinal and transverse correlation functions can be expected to be momentum dependent. Low-energy particles may be emitted on such long time scales that sensitivity to antisymmetrization effects is lost. As emission time scales decrease for more energetic emissions, differences between longitudinal and transverse correlation functions may become more significant for particle pairs of higher total momenta. These qualitative expectations are corroborated by the calculations shown in Fig. 18. The solid and dashed curves show longitudinal and transverse correlation functions predicted for narrow gates on the total momentum,  $P_{\text{c.m.}} = 300, 400,$

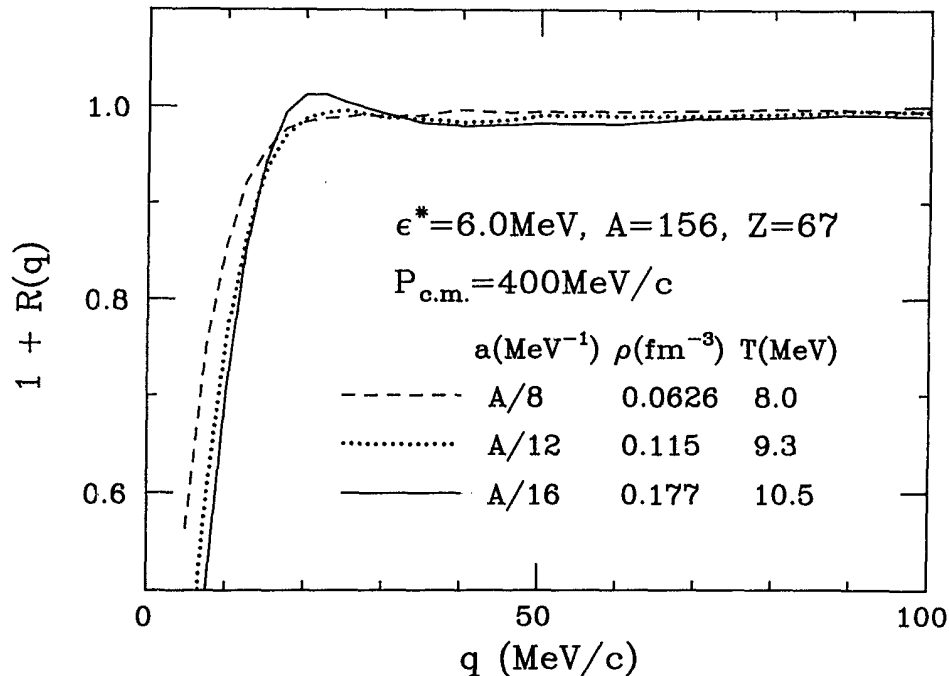


FIG. 16. Sensitivity of calculated two-proton correlation functions to different assumptions on the level density parameter,  $a = E^*/T^2$ , for the decay of  $^{156}\text{Ho}$  compound nuclei of initial excitation energy  $\epsilon^* = E^*/A = 6$  MeV.

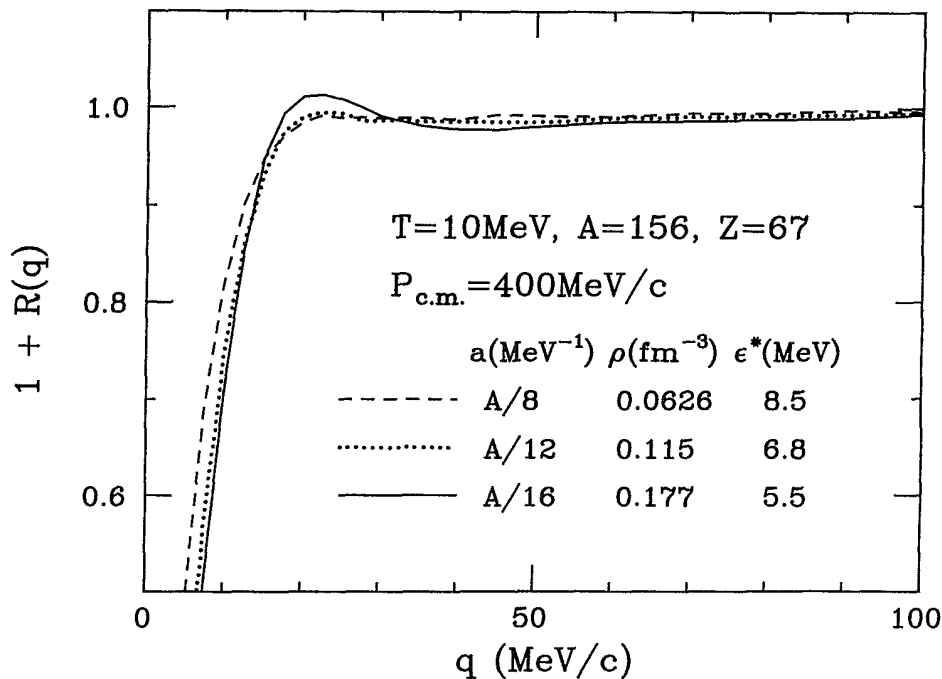


FIG. 17. Sensitivity of calculated two-proton correlation functions to different assumptions on the level density parameter,  $a = E^*/T^2$ , for the decay of  $^{156}\text{Ho}$  compound nuclei of initial temperature  $T = 10$  MeV.

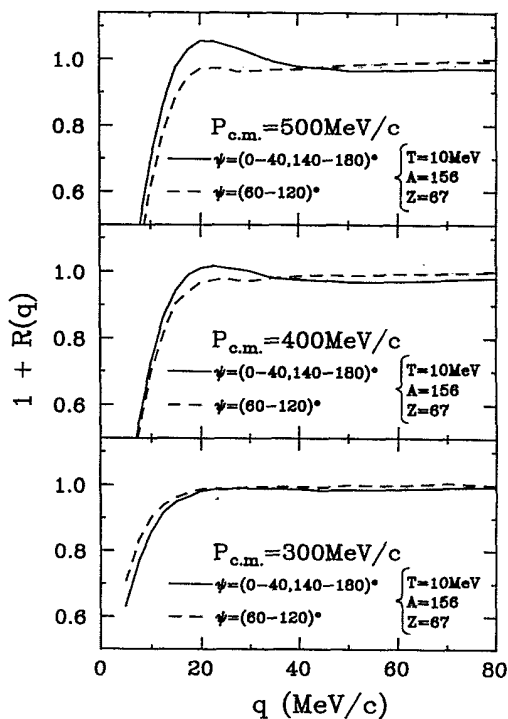


FIG. 18. Longitudinal and transverse correlation functions predicted for evaporative emission from  $^{156}\text{Ho}$  compound nuclei of initial temperature  $T = 10$  MeV. Different panels show predictions for different total momenta  $P_{\text{c.m.}}$  of the emitted proton pairs:  $P_{\text{c.m.}} = 500$  MeV/c (top panel),  $P_{\text{c.m.}} = 400$  MeV/c (center panel),  $P_{\text{c.m.}} = 300$  MeV/c (bottom panel).

500 MeV/c, of the particle pair with respect to the center-of-mass frame of reference (i.e., the rest frame of the compound nucleus). Significant differences between longitudinal and transverse correlation functions are predicted for large momenta,  $P_{\text{c.m.}} = 500$  MeV/c (top panel). These differences are reduced for smaller momenta,  $P_{\text{c.m.}} = 400$  MeV/c (center panel). For even smaller momenta,  $P_{\text{c.m.}} = 300$  MeV/c, longitudinal and transverse correlation functions differ only in the detailed shape of the minimum at  $q \approx 0$  MeV/c (bottom panel), which is more pronounced for the longitudinal than for the transverse correlation function.

## VIII. SUMMARY AND CONCLUSION

We have presented a general formalism allowing the calculation of two-proton correlation functions for any reaction model capable of predicting the one-body phase-space distribution of the emitted particles. We demonstrated the sensitivity of two-proton correlation functions to the space-time geometry of the emitting system via calculations for schematic emission sources, as well as for more realistic models of compound and precompound light particle emissions.

Particle emission from equilibrated compound nuclei typically proceeds on such long time scales that antisymmetrization and nuclear interaction between the two emitted particles play a relatively minor role. The correlation functions are dominated by final-state Coulomb interactions and exhibit only moderate sensitivity to details of the calculations. Once emission times are of the order of 100 fm/c or less, antisymmetrization effects and nu-

clear and Coulomb interactions must all be incorporated into the calculations and the correlation functions become rather sensitive to details of the space-time evolution of the reaction zone. The BUU calculations indicate considerable sensitivity of the predicted correlation functions to the magnitude of the in-medium nucleon-nucleon cross sections employed in these calculations. Small differences are predicted between transverse and longitudinal correlation functions which could be explored for further testing of reaction models. Considerable sensitivity is predicted for measurements which explore the dependence of the two-proton correlation function on the collision impact parameter and on the total momenta of the emitted proton pairs.

In our BUU calculations, we have seen very little sensitivity to the compressibility of nuclear matter. This is not surprising, since compressional effects are not yet very important at beam energies of 75 MeV/nucleon. In principle, one should also study the effects of a momentum-dependent mean field.<sup>41-44</sup> Such effects are expected to be important at higher beam energies ( $E/A \approx 1$  GeV). At these energies, it has been shown<sup>44</sup> that the effects of the momentum dependence of the mean field on the collective nuclear matter flow can be approximated by a momentum-independent mean field with a suitably changed compressibility. The same effect has been found at intermediate beam energies ( $E/A = 50-150$  MeV), where it was found that the disappear-

ance of nuclear collective flow could be reproduced by using a momentum-dependent mean field with a compressibility of 210 MeV (Ref. 45) or, alternatively, a momentum-independent mean field with a slightly higher compressibility of 240 MeV.<sup>46</sup> The investigations of Ref. 46 corroborate our present finding that fast particle emission in intermediate-energy nucleus-nucleus collisions ( $E/A \approx 50-150$  MeV) depends sensitively on the magnitude of the in-medium nucleon-nucleon cross sections, but only very little on the nuclear compressibility.

It is clearly desirable to extend future studies of two-proton intensity interferometry to higher beam energies ( $E/A \approx 1$  GeV) and to heavier projectile-target combinations. Such studies may provide additional insight into the momentum dependence and compressibility of nuclear matter, which could not be gained in an unambiguous fashion from observables tested so far.

#### ACKNOWLEDGMENTS

The authors would like to acknowledge helpful discussions with G. J. Kunde. This work is based upon work supported by the National Science Foundation under Grant Nos. PHY-89-13813, PHY-89-06116, and PHY-88-1439. S.P. gratefully acknowledges additional support from the Wisconsin Alumni Research Foundation and from the National Superconducting Cyclotron Laboratory.

<sup>1</sup>For a recent review, see, e.g., D. H. Boal, C. K. Gelbke, and B. K. Jennings, *Rev. Mod. Phys.* **62**, 553 (1990).

<sup>2</sup>S. E. Koonin, *Phys. Lett.* **70B**, 43 (1977).

<sup>3</sup>F. Zarbakhsh, A. L. Sagle, F. Brochard, T. A. Mulera, V. Perez-Mendez, R. Talaga, I. Tanihata, J. B. Carroll, K. S. Ganezer, G. Igo, J. Oostens, D. Woodard, and R. Sutter, *Phys. Rev. Lett.* **46**, 1268 (1981).

<sup>4</sup>W. G. Lynch, C. B. Chitwood, M. B. Tsang, D. J. Fields, D. R. Klesch, C. K. Gelbke, G. R. Young, T. C. Awes, R. L. Ferguson, F. E. Obenshain, F. Plasil, R. L. Robinson, and A. D. Panagiotou, *Phys. Rev. Lett.* **51**, 1850 (1983).

<sup>5</sup>H. A. Gustafsson, H. H. Gutbrod, B. Kolb, H. Löhner, B. Ludewigt, A. M. Poskanzer, T. Renner, H. Riedesel, H. G. Ritter, A. Warwick, F. Weik, and H. Wieman, *Phys. Rev. Lett.* **53**, 544 (1984).

<sup>6</sup>C. B. Chitwood, J. Aichelin, D. H. Boal, G. Bertsch, D. J. Fields, C. K. Gelbke, W. G. Lynch, M. B. Tsang, J. C. Shillcock, T. C. Awes, R. L. Ferguson, F. E. Obenshain, F. Plasil, R. L. Robinson, and G. R. Young, *Phys. Rev. Lett.* **54**, 302 (1985).

<sup>7</sup>B. K. Jennings, D. H. Boal, and J. C. Shillcock, *Phys. Rev. C* **33**, 1303 (1986).

<sup>8</sup>D. H. Boal and J. C. Shillcock, *Phys. Rev. C* **33**, 549 (1986).

<sup>9</sup>C. B. Chitwood, C. K. Gelbke, J. Pochodzalla, Z. Chen, D. J. Fields, W. G. Lynch, R. Morse, M. B. Tsang, D. H. Boal, and J. C. Shillcock, *Phys. Lett. B* **172**, 27 (1986).

<sup>10</sup>Z. Chen, C. K. Gelbke, J. Pochodzalla, C. B. Chitwood, D. J. Fields, W. G. Lynch, and M. B. Tsang, *Phys. Lett. B* **186**, 280 (1987).

<sup>11</sup>Z. Chen, C. K. Gelbke, W. G. Gong, Y. D. Kim, W. G. Lynch, M. R. Maier, J. Pochodzalla, M. B. Tsang, F. Saint-

Laurent, D. Ardouin, H. Delagrangé, H. Doubre, J. Kasagi, A. Kyanowski, A. Péghaire, J. Péter, E. Rosato, G. Bizard, F. Lefèbvres, B. Tamain, J. Québert, and Y. P. Viyogi, *Phys. Rev. C* **36**, 2297 (1987).

<sup>12</sup>J. Pochodzalla, C. K. Gelbke, W. G. Lynch, M. Maier, D. Ardouin, H. Delagrangé, H. Doubre, C. Grègoire, A. Kyanowski, W. Mittag, A. Péghaire, J. Péter, F. Saint-Laurent, B. Zwieglinski, G. Bizard, F. Lefèbvres, B. Tamain, J. Québert, Y. P. Viyogi, W. A. Friedman, and D. H. Boal, *Phys. Rev. C* **35**, 1695 (1987).

<sup>13</sup>J. Pochodzalla, C. B. Chitwood, D. J. Fields, C. K. Gelbke, W. G. Lynch, M. B. Tsang, D. H. Boal, and J. C. Shillcock, *Phys. Lett. B* **174**, 36 (1986).

<sup>14</sup>S. Pratt and M. B. Tsang, *Phys. Rev. C* **36**, 2390 (1987).

<sup>15</sup>D. Fox, D. A. Cebra, J. Karn, C. Parks, A. Pradhan, A. Vander Molen, J. van der Plicht, G. D. Westfall, W. K. Wilson, and R. S. Tickle, *Phys. Rev. C* **38**, 146 (1988).

<sup>16</sup>T. C. Awes, R. L. Ferguson, F. E. Obenshain, F. Plasil, G. R. Young, S. Pratt, Z. Chen, C. K. Gelbke, W. G. Lynch, J. Pochodzalla, and H. M. Xu, *Phys. Rev. Lett.* **61**, 2665 (1988).

<sup>17</sup>P. A. DeYoung, M. S. Gordon, Xiu qin Lu, R. L. McGrath, J. M. Alexander, D. M. de Castro Rizzo, and L. C. Vaz, *Phys. Rev. C* **39**, 128 (1989).

<sup>18</sup>D. A. Cebra, W. Benenson, Y. Chen, E. Kashy, A. Pradhan, A. Vander Molen, G. D. Westfall, W. K. Wilson, D. J. Morrissey, R. S. Tickle, R. Korteling, and R. L. Helmer, *Phys. Lett. B* **227**, 336 (1989).

<sup>19</sup>S. E. Koonin, W. Bauer, and A. Schäfer, *Phys. Rev. Lett.* **62**, 1247 (1989).

<sup>20</sup>J. Québert, R. Boisgard, P. Lautridou, D. Ardouin, D. Durand, D. Goujdami, F. Guibault, C. Lebrun, R. Tamisier,

- A. Pégahaire, and F. Saint-Laurent, in *Proceedings of the Symposium on Nuclear Dynamics and Nuclear Disassembly, Dallas, 1989*, edited by J. B. Natowitz (World Scientific, Singapore, 1989), p. 337.
- <sup>21</sup>D. Ardouin, F. Guilbault, C. Lebrun, D. Ardouin, S. Pratt, P. Lautridou, R. Boisgard, J. Québert, and A. Pégahaire, University of Nantes, Internal Report LPN-89-02.
- <sup>22</sup>P. A. DeYoung, C. J. Gelderloos, D. Kortering, J. Sarafa, K. Zienert, M. S. Gordon, B. J. Fineman, G. P. Gilfoyle, X. Lu, R. L. McGrath, D. M. de Castro Rizzo, J. M. Alexander, G. Auger, S. Kox, L. C. Vaz, C. Beck, D. J. Henderson, D. G. Kovar, and M. F. Vineyard, *Phys. Rev. C* **41**, R1885 (1990).
- <sup>23</sup>W. G. Gong, C. K. Gelbke, N. Carlin, R. T. de Souza, Y. D. Kim, W. G. Lynch, T. Murakami, G. Poggi, D. Sanderson, M. B. Tsang, H. M. Xu, D. E. Fields, K. Kwiatkowski, R. Planeta, V. E. Viola, Jr., S. J. Yennello, and S. Pratt, *Phys. Lett. B* **246**, 21 (1990).
- <sup>24</sup>W. G. Gong, C. K. Gelbke, N. Carlin, R. T. de Souza, Y. D. Kim, W. G. Lynch, T. Murakami, G. Poggi, D. Sanderson, M. B. Tsang, H. M. Xu, D. E. Fields, K. Kwiatkowski, R. Planeta, V. E. Viola, Jr., S. J. Yennello, and S. Pratt, *Phys. Rev. C* (to be published).
- <sup>25</sup>W. A. Friedman and W. G. Lynch, *Phys. Rev. C* **28**, 16 (1983).
- <sup>26</sup>D. H. Boal and H. DeGuise, *Phys. Rev. Lett.* **57**, 2901 (1986).
- <sup>27</sup>S. Pratt, *Phys. Rev. Lett.* **53**, 1219 (1984).
- <sup>28</sup>A. Messiah, *Quantum Mechanics* (North-Holland, Amsterdam, 1976), Vol. 1 (Appendix).
- <sup>29</sup>R. V. Reid, Jr., *Ann. Phys. (N.Y.)* **50**, 411 (1968).
- <sup>30</sup>L. W. Nordheim, *Proc. R. Soc. London* **A119**, 689 (1928).
- <sup>31</sup>C. Y. Wong, *Phys. Rev. C* **25**, 1460 (1982).
- <sup>32</sup>M. B. Tsang, W. G. Lynch, C. B. Chitwood, D. J. Fields, D. R. Klesch, C. K. Gelbke, G. R. Young, T. C. Awes, R. L. Ferguson, F. E. Obenshain, F. Plasil, and R. L. Robinson, *Phys. Lett.* **148B**, 265 (1984).
- <sup>33</sup>C. B. Chitwood, D. J. Fields, C. K. Gelbke, D. R. Klesch, W. G. Lynch, M. B. Tsang, T. C. Awes, R. L. Ferguson, F. E. Obenshain, F. Plasil, R. L. Robinson, and G. R. Young, *Phys. Rev. C* **34**, 858 (1986).
- <sup>34</sup>W. Bauer, *Nucl. Phys.* **A471**, 604 (1987).
- <sup>35</sup>W. Bauer, G. D. Westfall, D. Fox, and D. Cebra, *Phys. Rev. C* **37**, 664 (1988).
- <sup>36</sup>D. Ardouin, Z. Basrak, P. Schuck, A. Pégahaire, F. Saint-Laurent, H. Delagrange, H. Doubre, C. Grégoire, A. Kyanowski, W. Mittig, J. Péter, Y. P. Viyogi, J. Québert, C. K. Gelbke, W. G. Lynch, M. Maier, J. Pochodzalla, G. Bizard, F. Lefebvres, B. Tamain, B. Remaud, and F. Sébille, *Nucl. Phys.* **A514**, 564 (1990).
- <sup>37</sup>G. F. Bertsch, H. Kruse, and S. Das Gupta, *Phys. Rev. C* **29**, 673 (1984).
- <sup>38</sup>G. F. Bertsch and S. Das Gupta, *Phys. Rep.* **160**, 189 (1988).
- <sup>39</sup>A. detailed account of the numerical details is given in W. Bauer, Michigan State University Report MSUCL-699, submitted to *Phys. Rev. C*.
- <sup>40</sup>J. P. Bondorf, J. N. De, G. Fai, A. O. T. Karvinen, B. Jacobsson, and J. Randrup, *Nucl. Phys.* **A333**, 285 (1980).
- <sup>41</sup>C. Gale, G. F. Bertsch, and S. Das Gupta, *Phys. Rev. C* **35**, 1666 (1987).
- <sup>42</sup>J. Aichelin, A. Rosenhauer, G. Peilert, H. Stöcker, and W. Greiner, *Phys. Rev. Lett.* **58**, 1926 (1987).
- <sup>43</sup>G. Welke, M. Prakash, T. T. S. Kuo, S. Das Gupta, and C. Gale, *Phys. Rev. C* **38**, 2101 (1988).
- <sup>44</sup>For additional reference see *The Nuclear Equation of State*, Vol. 216A of *NATO Advanced Study Institute Series B: Physics*, edited by W. Greiner and H. Stöcker (Plenum, New York, 1990).
- <sup>45</sup>D. Krofcheck, W. Bauer, G. M. Crawley, C. Djalali, S. Howden, C. A. Ogilvie, A. Vander Molen, G. D. Westfall, W. K. Wilson, R. S. Tickle, and C. Gale, *Phys. Rev. Lett.* **63**, 2028 (1989).
- <sup>46</sup>C. A. Ogilvie, W. Bauer, D. A. Cebra, J. Clayton, S. Howden, J. Karn, A. Nadasen, A. Vander Molen, G. D. Westfall, W. K. Wilson, and J. S. Winfield, *Phys. Rev. C* **42**, R10 (1990).